Characterization of the Hamamatsu S12642-1616PA silicon photomultiplier with the newest generation of TARGET ASIC

Bachelorarbeit aus der Physik

Vorgelegt von
Manuel Loos
17.01.2017

Erlangen Centre for Astroparticle Physics
Physikalisches Institut II
Friedrich-Alexander-Universität Erlangen-Nürnberg

1. Gutachter: Prof. Dr. Stefan Funk
2. Gutachter: Prof. Dr. Gisela Anton

Abstract

Gamma-ray astronomy is a young field of research. Observing astronomical objects that emit those high energetic photons ($> 500\,\mathrm{keV}$) has only been possible since the 1960s with the help of satellites. By doing these observations, the most powerful events in the universe (e.g. supernovae, **A**ctive **g**alactic **n**uclei) can be studied. Since the last few decades, indirect, earthbound observations of gamma-ray photons with the help of Cherenkov flashes became possible. Here, the most recent scientific project is called **C**herenkov **T**elescope **A**rray (CTA) which will improve upon the sensitivity of previous Cherenkov telescopes like H.E.S.S. by an order of magnitude. For the faint and short ($\gtrsim 5\,\mathrm{ns}$) flashes, the telescope camera requires fast read out electronics and a photosensitive sensor. For the new camera design CHEC-S, TARGET read out electronic and silicon photomultipliers (SiPM) as photosensors are used. Since this high innovative camera prototype has not been built yet, a test of the full read out chain is performed within the scope of this thesis. The trigger performance of T5TEA was tested with triggerscans. It turned out that triggering is possible down to 1 p.e. (i.e. $\sim 4\,\mathrm{mV}$). Furthermore, the datapath of TARGET C has been tested by charge determination of each SiPM event. It turned out that measuring the area of each pulse yields best results. It also became apparent that calibration of the storage array capacitors is essential. With this calibration, first time pulse height spectra were recorded with TARGET under real conditions. The charge resolution up to the 8. p.e. was approximately two times better than the CTA requirements. In addition, some of the parameters of the used Hamamatsu SiPM have been characterized with the TARGET ASIC and with a oscilloscope as a reference.

Contents

1 Introduction

Astronomy was one of the first practiced natural sciences in history. Observing the huge universe has always been of great interest for mankind. At first, only the optical part of the electromagnetic spectrum was observable because telescopes that are sensitive to optical light are relatively easy to realize. In the 17. century, Galileo Galilei was the first to build an optical telescope which enabled a deeper more detailed look into space. Up to now, there had been a large technical progress in astronomy. Larger telescopes with higher light collection ability were realized. Furthermore, the whole electromagnetic spectrum of the universe became observable which made it possible to study the full range of astronomic phenomena. Observing e.g. the electromagnetic spectrum at energies larger than 500 keV (gamma-rays) is useful to study the most powerful events in the universe. The gamma-ray can either have a thermal or non-thermal origin. Up to now, no object is known (apart from Big Bang) that emits gamma-rays only due to black body radiation[1]. Another (non-thermal) process to create gamma rays in the universe is Compton up-scattering. In this process, a high energy charged particle (i.e. proton, electron) interacts with a photon and thus transfers some of its energy to the photon. Furthermore, a charged particle can be accelerated, e.g. due to magnetic fields. The last important process which leads to emission of gamma-rays is the decay of a neutral pion which has been observed in supernova remnants [2]. Furthermore, possible astronomic sources which emit gamma-rays are neutron stars or Active Galactic Nuclei[2] (AGNs). Even the, not yet discovered, decay of hypothetical Dark Matter can lead to gamma ray emission.
By observing the universe in the gamma spectrum, one can trace populations of high energy particles which can not be observed directly. [1, 4]

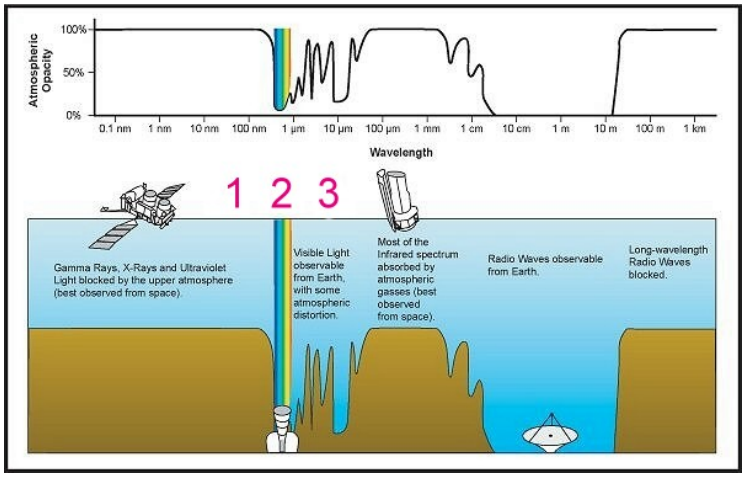

Figure 1: Absorption of electromagnetic radiation in earths atmosphere[5]

[1] isotropic thermal radiation, reflects temperature of emitting body[1]
[2] super-massive black hole ($M_{BH} < 10^{10} M_{Sun}$) in center of a active galaxy[3]

Gamma rays can only be observed directly with a satellite since the high energetic photons are absorbed in the atmosphere, as seen in Figure 1. Gamma satellites such as INTEGRAL (International Gamma-Ray Astrophysics Laboratory) use the effect that gamma rays interact with scintillating detector material. The thus emitted light flashes are detected with a photomultiplier. The flux of gamma photons decreases with rising photon energy ($\sim E^{-2.7}$[6]). Since the detector area of a satellite is limited due to technical restrictions, the effective detection area at very high energies is small.
Thus, a different approach has been followed. Gamma rays interact with the atmosphere and create a Cherenkov light which can be detected with earthbound Imaging Atmospheric Cherenkov Telescopes (IACTs). In 1989, the 10 m Whipple telescope was the first to detect the gamma-ray emission of an astronomical object (Crab Nebula) [7].
Apart from existing projects like H.E.S.S (High Energy Stereoscopic System), a novel observatory called Cherenkov Telescope Array (CTA) is in development. In the upcoming chapters, an introduction to Cherenkov flashes as well as the CTA project will be given.

2 Cherenkov Telescope Array

2.1 Cherenkov flashes

When Very High Energy (VHE) photons ($E > 100\,GeV$) enter the atmosphere, electron-positron-pairs can be produced in the vicinity of an atmospheric nuclei. Both leptons are decelerated in the atmosphere matter and thus produce Bremsstrahlung [8, p. 254]. This secondary photon can again produce a electron positron pair and so on. This process continues until the energy of the produced Bremsstrahlung photon is not sufficient to create electron-positron-pairs and the so called electromagnetic cascade ends.

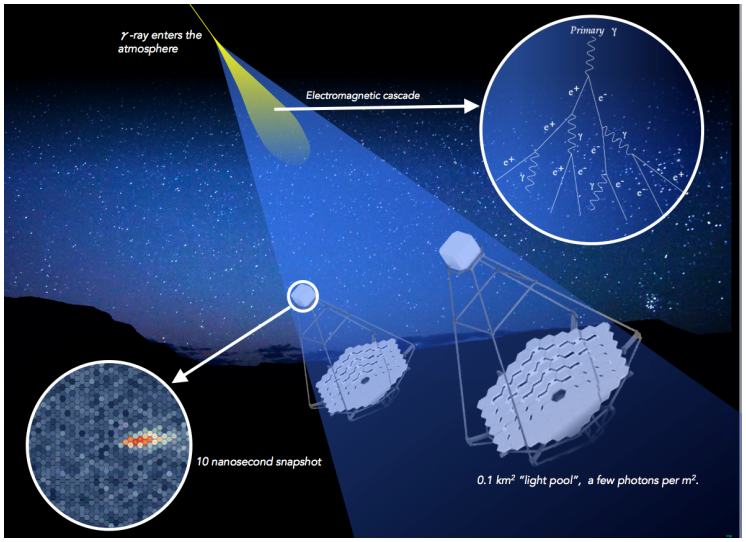

Figure 2: Formation of Cherenkov flashes caused by incoming gamma photon[9]

Due to the high energy of the initial photon, the charged particles can travel faster than the local speed of light[3] c. This leads to the emission of Cherenkov light which has a blue color. All the light of the cascade is emitted within a few nanoseconds, thus can be referred to as a Cherenkov flash. These flashes can be detected with a IACT by focusing the light onto a plane of photosensors with a mirror (see Figure 2) [1, 10, 11].

2.2 Introduction to project CTA

The overall aim of CTA is to cover the large energy range of 30 GeV-300 TeV while improving the sensitivity by an order of magnitude compared to current IACTs like H.E.S.S..
Therefore, IACTs with different size are grouped together to an array. To cover the whole sky, one array is planned for the northern hemisphere (La Palma, Spain) and the other array is planned for the southern hemisphere (Paranal, Chile). Figure 3 shows the proposed layout for both arrays.

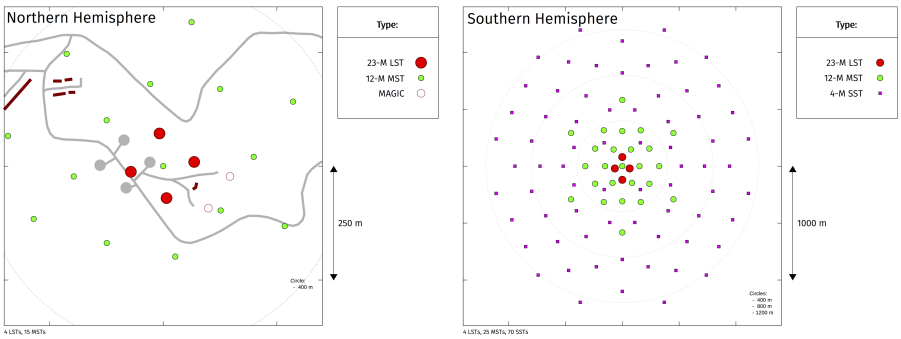

Figure 3: Proposed array layout for northern and southern hemisphere [9]

Three different telescope sizes are proposed. They cover different parts of the electromagnetic spectrum. The Large Size Telescope (LST) has a mirror diameter of $\sim 23\,\mathrm{m}$ and covers lower energy events. Since the gamma flux is indirect proportional to gamma energy, only 4 LSTs are proposed for the northern and southern hemisphere. The LSTs have to be large to collect enough light of the Cherenkov flashes that are faint due to low gamma energy.
The Medium Size Telescope (MST) has a diameter of $\sim 12\,\mathrm{m}$. 15 MSTs are proposed for the northern and 25 MSTs are proposed for the southern hemisphere. They are spread over an area of $\sim 1\mathrm{km}^2$ which improves the sensitivity in the 100 GeV-10 TeV range by a factor of ten.[12, 13]
The Small Size Telescope (SST) has a diameter of $\sim 4\,\mathrm{m}$. 70 SSTs are proposed for the southern hemisphere, covering $\sim 10\mathrm{km}^2$. This high detection area ensures that enough rare Cherenkov flashes, initiated by highest energy photons, are detected. Since Cherenkov

[3] $c = \frac{c_0}{n}$ where n is the refractive index of the surrounding medium and c_0 is the vacuum speed of light

light, initiated by multi-TeV photons, are rather "bright" the IACTs do not have to be very large to collect enough light. SSTs cover the energy range from few TeV up to over 100 TeV [9, 14, 15].

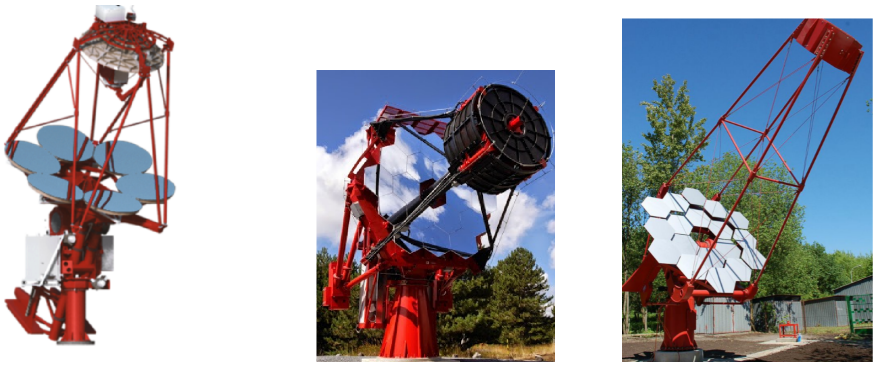

(a) GCT design. **(b)** ASTRI design. **(c)** SST-1M design.

Figure 4: Proposed designs for SSTs [15, 9].

Several telescope designs were proposed for the SST. Two of them (**G**amma **C**herenkov **T**elescope, **A**strophysics con **S**pecchi a **T**ecnologia **R**eplicante **I**taliana) have a so called Schwarzschild-Couder design consisting of two mirrors. The other one (SST-1M) has a single-mirror Davies-Cotton design. In the two mirror design a secondary 2 m mirror is used. This design shortens the focal length from 5.6 m (SST-1M) to 2.28 m (GCT). Furthermore, both mirrors demagnify the air shower image which leads to a reduction of the camera size from 0.88 m (SST-1M) to 0.35 m (GCT) at a similar Field of View of $\sim 9°$. All three IACTs (see Figure 4) are proposed to have silicon photomultipliers (SiPMs) as photosensors. Since GCT is the only SST to have TARGET (TeV Array Readout with GSa/s sampling and Event Trigger) readout electronics, its camera is described further in next chapter [15, 16, 9].

2.3 Camera of GCT

As already stated, GCT is the only SST to have TARGET for digitization and triggering. There are two GCT camera prototypes. The first prototype that has been built was CHEC-M (Compact High Energy Camera) with Multi Anode Photo Multipliers (MAPMs) as a photosensor (see Figure 6). In 2015 this camera was installed on a GCT prototype in Paris. 12 Cherenkov events were observed which made the GCT with CHEC-M the first CTA telescope to detect Cherenkov flashes.
The next camera prototype is CHEC-S which uses a SiPM as a photosensor. Each of the 2048 pixels has a physical size of 6x6mm^2. Both cameras consist of 32 front-end electronics (FEE) modules. One FEE module for CHEC-M is shown in Figure 5. Each FEE module consists of:

- 64 pixel photosensor (MAPM, SiPM)
- preamplifier module
- digitization module (TARGET ASIC[4])

The preamplifier module consists of 4 PCBs[5] each processing 16 channels. It shapes[6] the analogue signal of each photosensor pixel in order to improve digitization. For triggering and digitization, four TARGET ASICs are used, each processing 16 channels. Four adjacent channels are grouped together (superpixel) for so called first level triggering which is processed by an FPGA[7]. If two adjacent superpixel have a trigger in a certain time intervall, the FPGA on the back-end electronics (BEE) initiates a camera-wide trigger which leads to readout a part of the storage array of all TARGET modules (see chapter 3.2). Two data acquisition (DACQ) boards route all data to the outside of the camera.

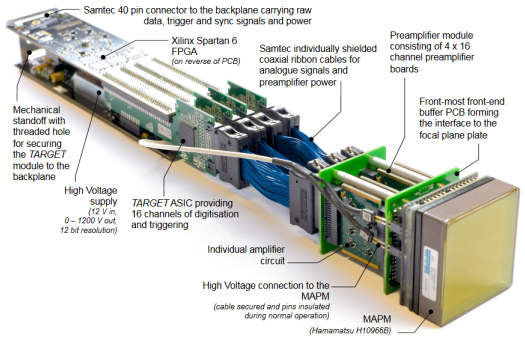

Figure 5: FEE module of the CHEC-M camera prototype [16]

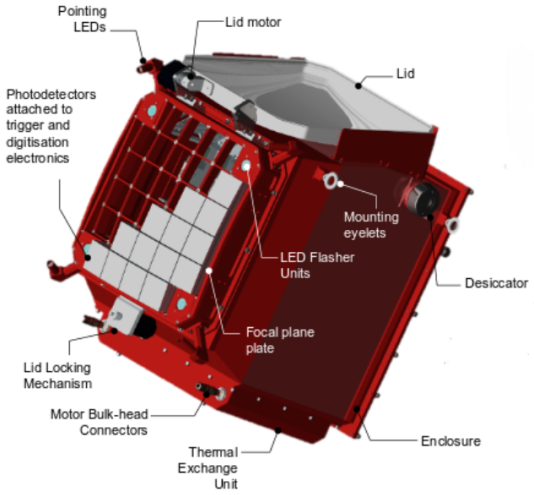

Figure 6: CHEC-M camera prototype (modified by author)

The CHEC-S prototype is currently being constructed. Apart from the different photosensor (SiPM) also the newest TARGET ASIC will be implemented. Furthermore, the preamplification has to be adapted to SiPMs.
SiPMs have the advantage over MAPMs, that they have a lower power consumption due to low operation voltage. Besides, SiPMs are generally cheaper than MAPMs and have a better performance per unit cost. Moreover, SiPMs can not be damaged by too much light, which makes observation at ambient light (moon) possible. One disadvantage is the

[4] **A**pplication-**S**pecific **I**ntegrated **C**ircuit
[5] **P**rinted **C**ircuit **B**oard
[6] 10%-90% rise time 3.5-6 ns; FWHM 5.5-10.5 ns[17]
[7] **F**ield **P**rogrammable **G**ate **A**rray

high dark count rate and the required temperature stability to have a constant gain (see chapter 5). Although crosstalk is always present, SiPMs are a reasonable alternative to generally used MAPMs [1, 14, 16].

Since CHEC-S has not been finished yet, testing the newest generation of TARGET ASIC on the preamplified and shaped SiPM signal would be useful. This testing is done within the scope of this thesis.

3 TARGET

The TARGET ASIC was designed to read out signals from Cherenkov cameras (e.g. CHEC, see chapter 2.3). The signal is sampled continuously with a high sample rate of 1 GSa/s which is fast enough for digitizing rather short signals (FWHM $< 10.5\,\mathrm{ns}$[17]). For each of the 16 channels, 16348 samples (i.e. $\sim 16\,\mu\mathrm{s}$) can be temporary stored and read out on demand. Triggering is done with T5TEA while TARGET C performs digitization.
With the help of many previous TARGET generations, one had figured out that separation of triggering and sampling in two different ASICs improves the trigger performance because it prevents that interferences from the data path jump over to trigger path [18, 19]. Figure 7 shows the evaluation board which was used throughout this thesis. It has all important components (T5TEA, TARGET C and an FPGA) in order test triggering and digitization of TARGET module.

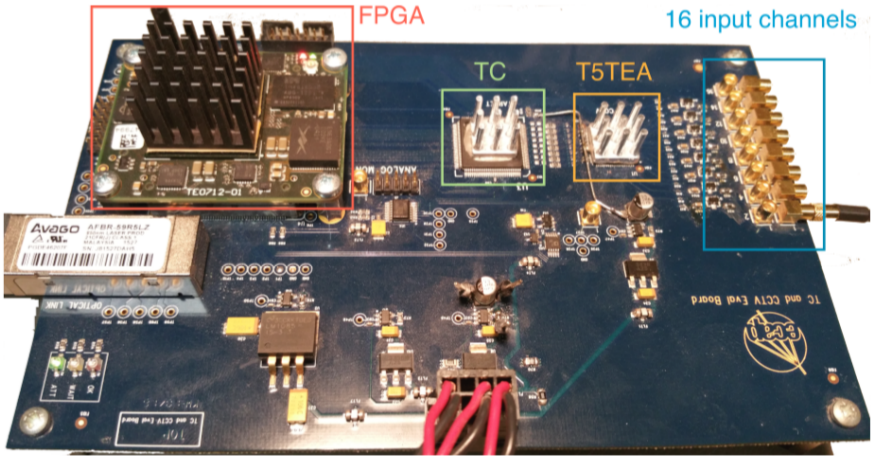

Figure 7: TARGET evaluation board [11]

3.1 T5TEA

T5TEA is used to trigger on the input signal. Therefore, four adjacent channels are grouped together by using the analog sum which is compared to a trigger threshold. The trigger process itself can then be configured with certain parameters which are set in 12 bit **D**igital to **A**nalog **C**onverter counts by the FPGA. An illustration of a successful trigger is shown in Figure 8.

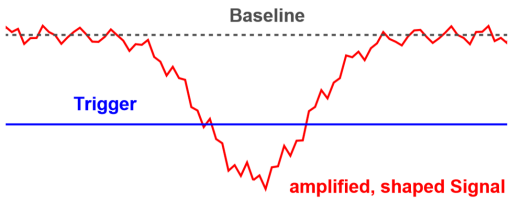

Figure 8: Illustration of the summed up signal position relative to the trigger threshold to achieve triggering. [11]

The three most important parameters are:

- TRG_Thres
- PMTref4
- Vped

The TRG_Thres parameter controls the trigger threshold of a trigger group. Increasing this parameter shifts the trigger towards the signal. The PMTref4 parameter controlls the signal offset of a triggergroup. Increasing of PMTref4 shifts the signal away from the threshold. Finally, there is Vped, which shifts the signal for each channel, counteracting to PMTref4.

3.2 TARGET C

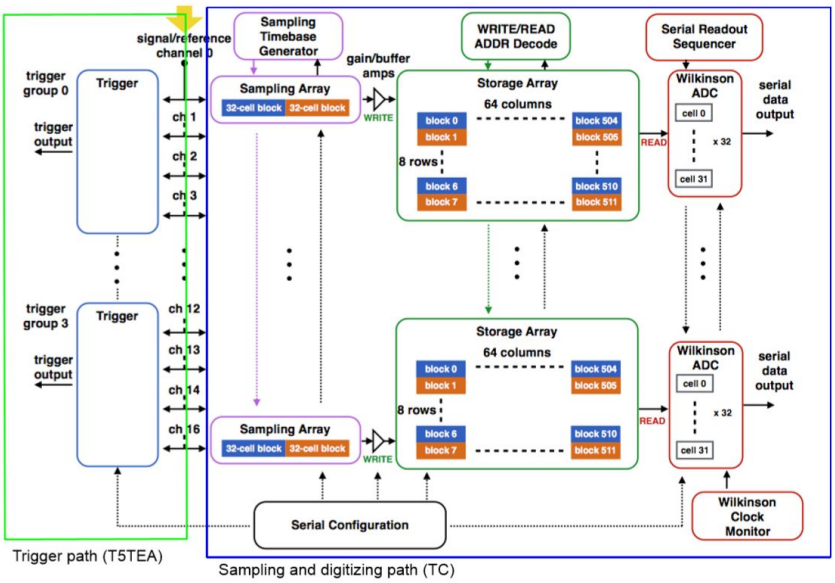

Figure 9: Schematics of trigger and data path of newest TARGET generation[20]

First, for each channel the signal is sampled in a 64-cell switched-capacitor array. The first 32-cell block is sampling while the other block is transfered to the storage array which consists of 512 32-cell blocks. In the next half cycle, the roles are reversed. This ping-pong fashion limits the input impedance and enables continuous sampling at large bandwidth (500 MHz for TARGET 5 [10]). The sampling process is controlled by a timebase generator which adjusts the time between each sample (from 1 ns to $\sim$ 2.5 ns) via an array of base delay elements. Samples that are stored in the buffer board are accessible in blocks of 32 samples on demand (e.g. if T5TEA applies trigger signal). The voltages in the storage capacitors are then digitized by 32 Wilkinson **a**nalog-to-**d**igital **c**onverter (ADC). Each ADC generates a voltage ramp and starts a 12 bit counter at the same time. If the ramp crosses the voltage that is stored in the capacitor, the counter stops. The counts then represents the cell voltage if the ramp voltage rises linear with time. Afterwards, the digitized samples of all 16 channels are then serially transfered further. Figure 9 shows the functionality of trigger path (left) and data path (right).

4 Experimental setup

In Figure 10 one can see the experimental setup. The Hamamatsu SiPM was put in a light-tight box together with a LED flasher which is called "Laser". At the back of the SiPM, the buffer board is located. The shaperboard was outside the box. Apart from the TARGET evaluation board (Figure 7), a MSO-X 3054A oscilloscope[8] from Agilent Technologies was used in chapter 5.2 and 6. Measurements with this oscilloscope can be taken as a reference for TARGET measurements due to higher sampling rate (see chapter 3 and 3.2) and better performance. Furthermore, the Keysight 33611A[9] wave generator was used in chapter 7.1.1,7.2.2 and 7.2.3.

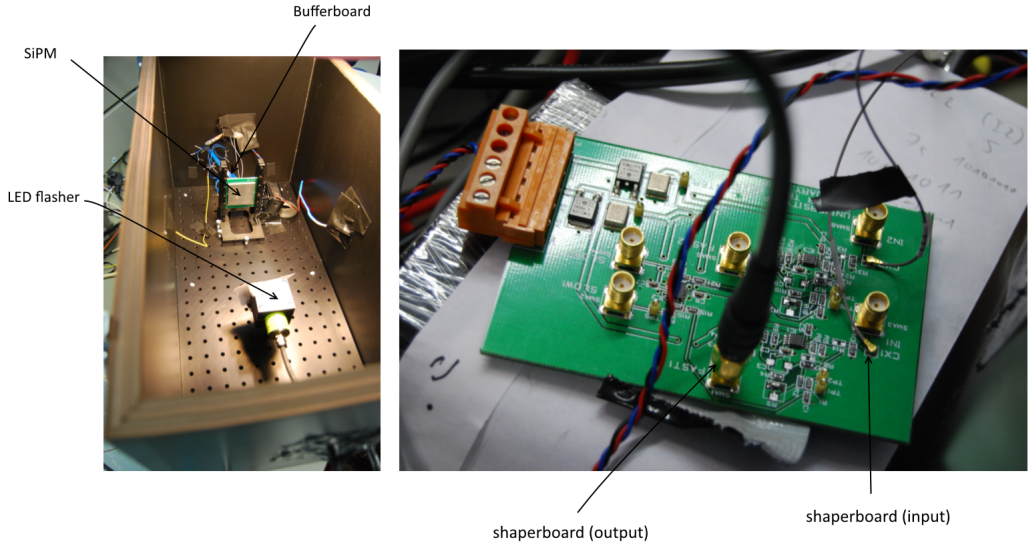

Figure 10: Picture of experimental setup (left) and shaperboard (right)

5 Silicon photomultiplier (SiPM)

Cherenkov flashes are rather faint and appear only in a very short time period ($\gtrsim 5\,\mathrm{ns}$) [10]. Silicon photomultiplier are most commonly used to convert the optical flash into an analogue electrical pulse. They are able to detect single photon events at good time response. Compared to conventional photomultiplier tubes (PMTs), SiPMs have several advantages. First of all, there is the insensitivity to magnetic fields to mention. Furthermore, SiPM detectors have a lower operation voltage (20 V-90 V, [23]) and have a light, compact design

[8] 500 MHz bandwidth, 4 GSa/s sampling rate [21]
[9] 80 MHz bandwidth, 660 MSa/s sample rate[22]

due to their functionality [24] (see 5.1).
In the following chapter 5.1 the technical functionality and characteristics of SiPMs are described. This helps to understand later measurements e.g. determination of gain (chapter 8.2). In chapter 5.2, the amplified and shaped SiPM signal was analyzed with the oscilloscope to get an overview of the signal itself.

5.1 Characteristics and functionality of SiPM

A silicon photomultiplier consists of 100 to 90000 avalanche photo diodes (APD), the so called APD matrix. Figure 11 shows the structure of an APD. Most commonly used is a p^+-i-p-n^+ structure where p stands for p doped silicon layer and n means n doped silicon layer. The + indicates an heavy doped layer. There is an electric field in the depletion region of the weak p doped intrinsic i-layer due to the external bias voltage. To intensify this electric field, a second p-doped layer is located between i and n^+ (see Figure 11). When one photon hits the intrinsic layer, it is getting absorbed by a silicon atom. An

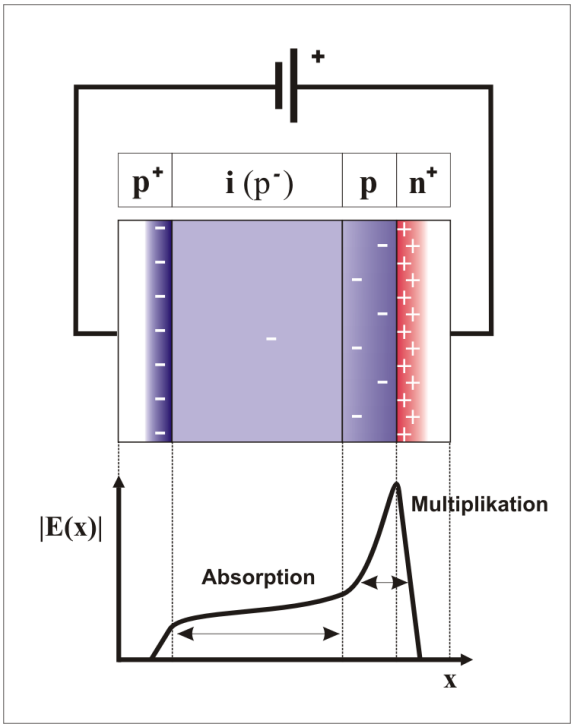

Figure 11: Schematics of an avalanche photodiode[25]

electron in the valence band can be lifted up to the conduction band which ionizes the atom. The resulting electron hole pair moves in opposite direction due to electric field. In the so called Multiplication Area between p and n^+ layer, the (photo)-electron is heavily accelerated due to the large electric field. This leads to a creation of multiple electron hole pairs due to impact ionization. The electron multiplication depends on the bias voltage. If

the voltage is smaller than the so called break down voltage, the multiplication is linear to the number of initial photo electrons. But if the bias voltage exceeds the break down voltage, the multiplication is avalanche-like. Then, the amplification μ ranges from 10^5 to 10^6 (bias voltage depend). Here, the avalanche-like process leads to the same signal, regardless of how much photons hit the APD. [26, 24, 23].
Due to non linearity of amplification, it is not possible to count the number of photon events with only one APD. Therefore, more APD have to be connected in parallel. If the number of expected photons per time interval is much less then the number of APD, one can assume that only one photon is absorbed in an APD at a time. The electrical current for each APD are added together which leads to an overall current that is proportional to the number of photons. Figure 12 shows an equivalent circuit diagram of two parallel-connected APDs with a bias voltage that is higher than the break down voltage. A single APD can be described with a capacitor C_j, an internal resistor R_S, a voltage source V_BD for the break down voltage and a switch S. As long as no photon is absorbed, S is open which leads to all capacitors C_j being charged with V_BIAS. At this moment, the APDs work in the so called Geiger mode. If one photon creates an avalanche (see above), S suddenly closes. C_j can now discharge through R_S which leads to a rising current. This APD current leads to an increasing voltage drop at the so called quenching resistor R_Q. If R_Q is high enough ($\gtrsim 100\,\mathrm{k\Omega}$ [27]), the voltage of C_j can fall below V_BD which quenches the avalanching process (S opens). At this time the APD current is maximal with $i_\mathrm{max} = \frac{V_\mathrm{BIAS} - V_\mathrm{BR}}{R_\mathrm{Q} + R_\mathrm{S}}$.
C_j can now recharge to V_BIAS over the quenching resistor R_Q. The current through the APD and R_Q (microcell) is decreasing exponentially to zero.

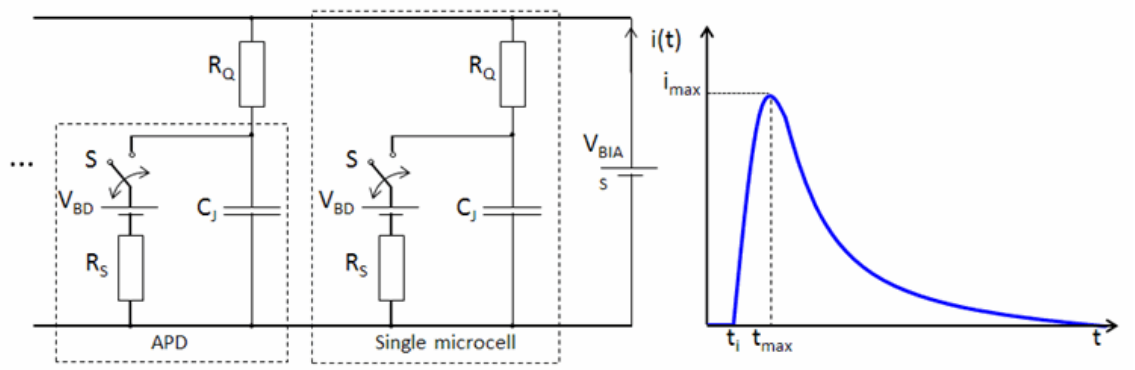

Figure 12: Process of generating a SiPM signal [28]

To get the total charge that passes the microcell, one has to integrate over the time-current curve in Figure 12. Due to additivity of the current for each microcell and the assumption from above, it is possible to determine the number of initial photo electrons by calculating the area of the signal [26] (see 6.2).
Figure 13 shows a possible design of the microcells within a SiPM.

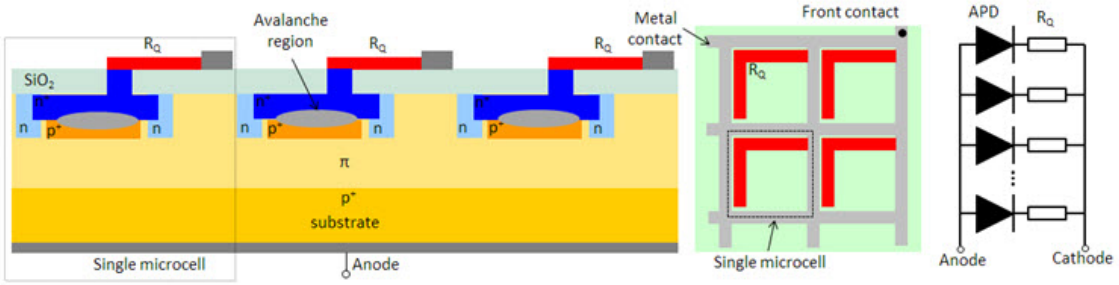

Figure 13: Layout of Hamamatsu silicon photomultiplier[29]

With the above explained functionality of a SiPM, it is possible to describe various effects e.g. so called dark counts.
Dark count events are events that are not caused by photons. Here, thermal noise of silicon atoms leads to creation of an electron hole pair with an avalanche which can not be distinguished from a photon triggered event. The number of dark counts per time (dark count rate) rises with temperature since the silicon atoms have more thermal energy to create electron hole pairs. Furthermore, the dark count rate rises with bias voltage V_{BIAS} since the electric field strengthens with rising V_{BIAS}. This decreases the required energy of an atom to produce electron hole pairs and thus increases the number of atoms that are able to become ionized. The dark count rate of SiPMs is very high ($\sim 1\,\mathrm{MHz}$ per mm^2 detector area)[24].
Additionally, one has to consider crosstalk. Due to this, the output signal can be higher than the signal produced by the incident light. This can be explained with additional photons that are created during an avalanche process (recombination of electron and holes). Typically, 10 photons are generated at each avalanche process [30]. If one photon hits the intrinsic layer of adjacent microcells, crosstalk occurs. That is why this effect always sophisticates the photon counting process.
In all following measurements, not only the raw SiPM signal was used. The signal was buffered with a buffer board. Here the output charge of the signal was transfered to a voltage and amplified from $0.2\,\mathrm{mV}$ per p.e. to $\sim 4\,\mathrm{mV}$[31]. The following shaper board shapes the signal. The width of the signal is reduced to prevent different signals from overlapping [32]. One important parameter of a SiPM is the so called gain which, in this case, describes the rise of the amplitude of the buffered and shaped SiPM signal with increasing photon electron number. The maximum current i_{max} of a microcell increases with rising V_{BIAS}. Due to additivity of current for all microcells, the maximum current of the whole SiPM is proportional to the number of photoelectrons. This proportionality is maintained after buffering and shaping the signal. The gain itself is therefore determined by the amplification of the buffer board and V_{BIAS}. For all following measurements, the bias voltage will be called SiPM voltage.

5.2 Display of SiPM signal on the oscilloscope

To better understand the SiPM signal it was at first analyzed with the oscilloscope. This measurement at the very beginning can be seen as a reference for later measurements with the TARGET evaluation board.
Viewing the SiPM output with the scope gives also the opportunity to study the signal for different input parameters. This can be for example the voltage or the intensity of the laser beam. Both can be adjusted in the experimental setup.
The characteristic peak in the signal appears non-periodically and is therefore intermittent. Therefore, one has to make use of a trigger which only displays the signal when certain conditions are met. Two different trigger methods are applied in the measurement:

- Trigger on signal
- Trigger on laser pulse

While triggering on the signal itself the waveform is only displayed if the voltage is higher than an adjustable trigger threshold. On the other hand one can trigger on the laser that emits pulsed light onto the SiPM. This laser is controlled via a trigger unit that is in turn connected to the wave generator of the oscilloscope. Every time the wave generator outputs a pulse, the laser emits a light beam on the falling edge of the incoming pulse. Thus, it is possible to trigger on the flashlight itself. Since the laser pulse is delayed in respect to the exact trigger point it is necessary to set a certain time delay in the scope. Even the length of the coax cable that connects the scope to the laser trigger unit and the associated light travel time cause a small but not negligible delay that has to be taken into account. In the experimental setup an empirically obtained delay of 89.28 ns was used. The horizontal and vertical range of the scope were set to 30 ns and 40 mV, respectively.

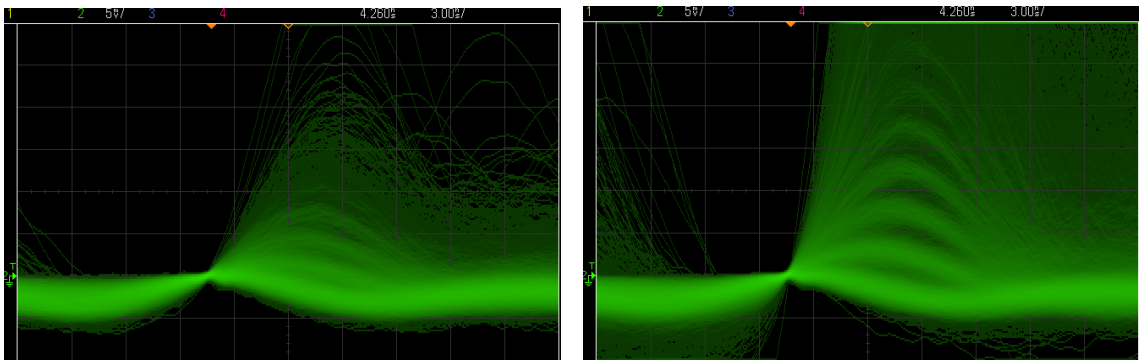

Figure 14: Buffered and shaped SiPM signal at 67.7 V (left) and 69.3 V (right) with 0 V threshold

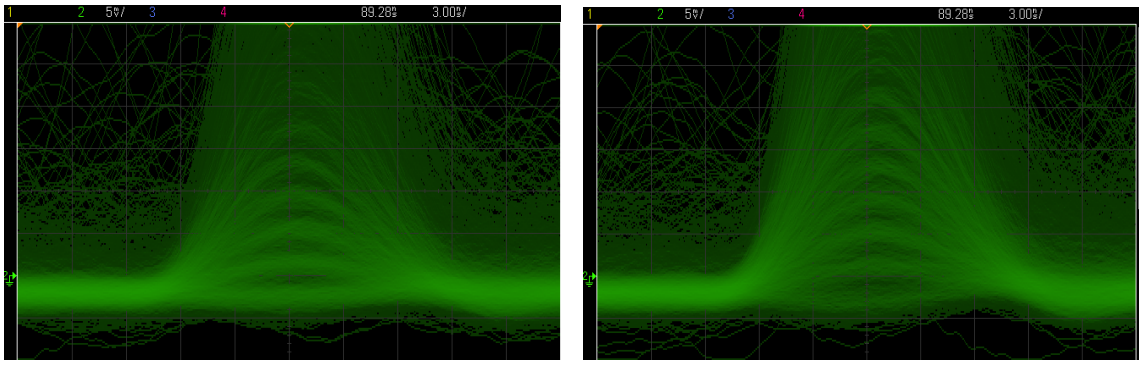

Figure 15: Buffered and shaped SiPM signal (trigger on laser) at 68.5 V with low- (left) and higher laser intensity (right)

As can be seen in Figure 14 and 15, most events have a particular, equidistant amplitude. Each cluster corresponds thereby to a photon event. The number of photons, which cause the event, and the number of released photoelectrons (p.e.) is proportional to the signal amplitude. The proportionality factor is also known as gain (see 5.1).
In Figure 14 one can see the influence of the SiPM voltage on the waveform itself. Both images ware taken with a threshold voltage of 0 V since the baseline has a negative electrical potential ($\approx -1.5\,\mathrm{mV}$). Increasing the SiPM voltage results in a larger amplitude separation and therefore higher gain.
Both screenshots in Figure 15 were taken at a constant SiPM voltage (68.5 V). Unlike the prior image, triggering occurs on the laser pulse which intensity was altered. Thus, there is no lower amplitude limit, which occurs only because of the threshold voltage, but rather a straight baseline. The higher the laser intensity the higher is the number of p.e..

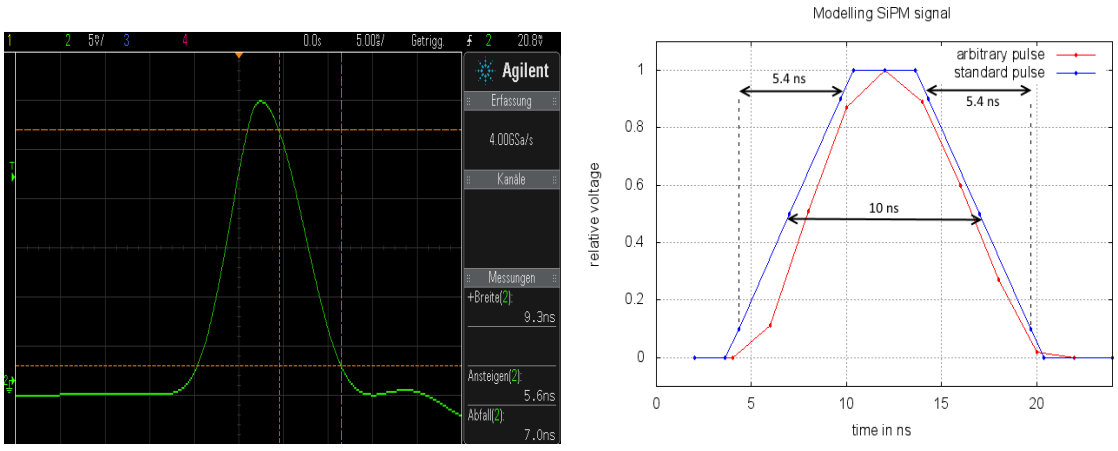

Figure 16: Average of amplified and shaped SiPM signal over many events (left) and signal modeling (right)

In Figure 7.2.2 the geometry of the signal has been further analyzed. The left picture shows the signal, averaged over 2000 events. The mean FWHM is 9.3 ns, the $10\% - 90\%$ leading and $90\% - 10\%$ falling edge is 5.6 ns and 7.0 ns, respectively. The right picture in Figure 7.2.2 shows the thus modeled signal in comparison to the standard pulse[10]. With this modeled signal it is possible to calibrate the TC storage array. This calibration and measurements with it on varying SiPM signals is done in 7.2.2 and 7.2.3.

The short overview of the SiPM signal and scope imaging provides a quick estimation of how the waveform looks like and how it behaves with changing parameters like laser intensity. It also helps to understand further measurements e.g. a triggerscan (see 6.1).

6 Determination of electrical charge

As explained in the previous chapter, the SiPM signal is separated into single photon events. Since the overall aim is to determine the number of p.e., which causes the pulse, one has to find another method than imaging. This can be done by measuring the amplitude.

6.1 Triggerscan for measuring the signal amplitude

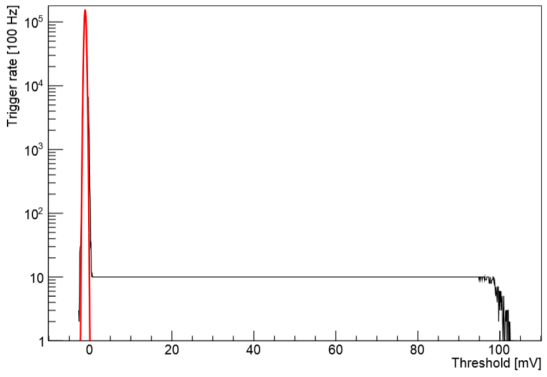

Figure 17: Triggerscan at constant amplitude [19]

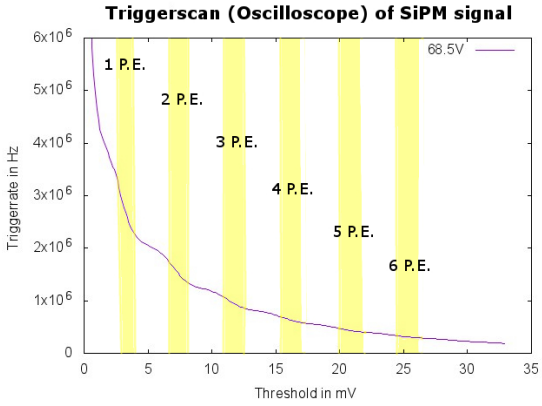

Figure 18: Triggerscan at variable amplitude like SiPM

During a triggerscan the triggerthreshold is varied in certain intervals. For each threshold the number of triggers per time (triggerrate) is measured. This can give a lot of information about the amplitude distribution of the waveforms.
In Figure 17 one can see such a triggerscan, performed on a pulse that has a constant amplitude. Here, the red fit shows the area where the threshold is in the noise of the baseline which leads to a fast increasing triggerrate.

[10] 10 ns FWHM, 5.4 ns edge time

In a bigger range (up to 100 mV, depending on the signal amplitude) the threshold is between the baseline and the top of the signal. The triggerrate is equal to the frequency of the pulse. If further increasing threshold voltage, the rate goes down to zero. The width of that drop depends on the noise performance of the measuring device or the noise on the signal.

In Figure 18 the triggerscan was performed with the oscilloscope and a variable source i.e. the SiPM. Unlike the scan with constant signal the triggerrate always decreases because some events are below that threshold and are not triggered on. Due to the photon events and the clustering at particular amplitudes the slope of the triggerrate curve is varying. If the threshold is passing a p.e. amplitude, then the rate is decreasing faster (lower slope) than if the threshold is right in between two adjacent p.e..

This method of measuring the amplitude distribution is very useful for determination of gain (see 8.2).

6.1.1 Variation of laser intensity

In this chapter the influence of the laser intensity on the amplitude distribution of the SiPM signal is tested. Therefore, a triggerscan at 68.5 V SiPM voltage was performed, once without - and once with “strong“ Laser. Since the laser intensity is changed in arbitrary units, “strong“ refers to an intensity where several photons hit the photosensor for each pulse. In Figure 19 one can see that the rate of each p.e. does not depend very much on laser intensity. That is because the dark count rate of this particular SiPM is so high ($\sim$ 6 MHz/pixel) [32]) that the laser that has a pulsing frequency (adjustable with a wave generator) of 250 kHz does not contribute a lot to the overall rate.

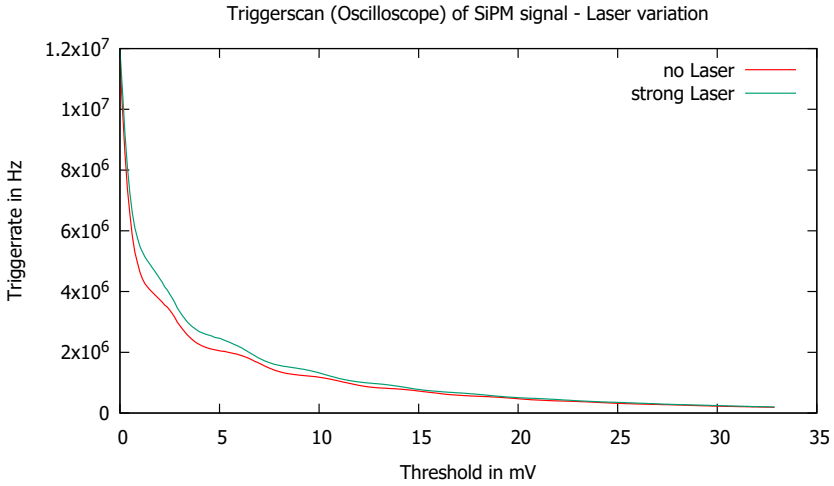

Figure 19: Triggerscan with and without strong laser

6.1.2 Variation of the SiPM voltage

A triggerscan was performed at different SiPM voltages ranging from 66.5 V to 69.7 V in 0.4 V steps (see figure 20). It can bee seen that from 67.7 V on the typical stepping shape starts to evolve. That is because the bias voltage starts getting higher than the break down voltage (67.6 V[32]). Furthermore, the effect of growing gain with SiPM voltage that was also seen in chapter 5 is observable since the steeper part of the curve is moving to higher threshold values at larger SiPM voltages. It is also easy to see that the overall triggerrate increases with SiPM voltage since the dark count rate rises.

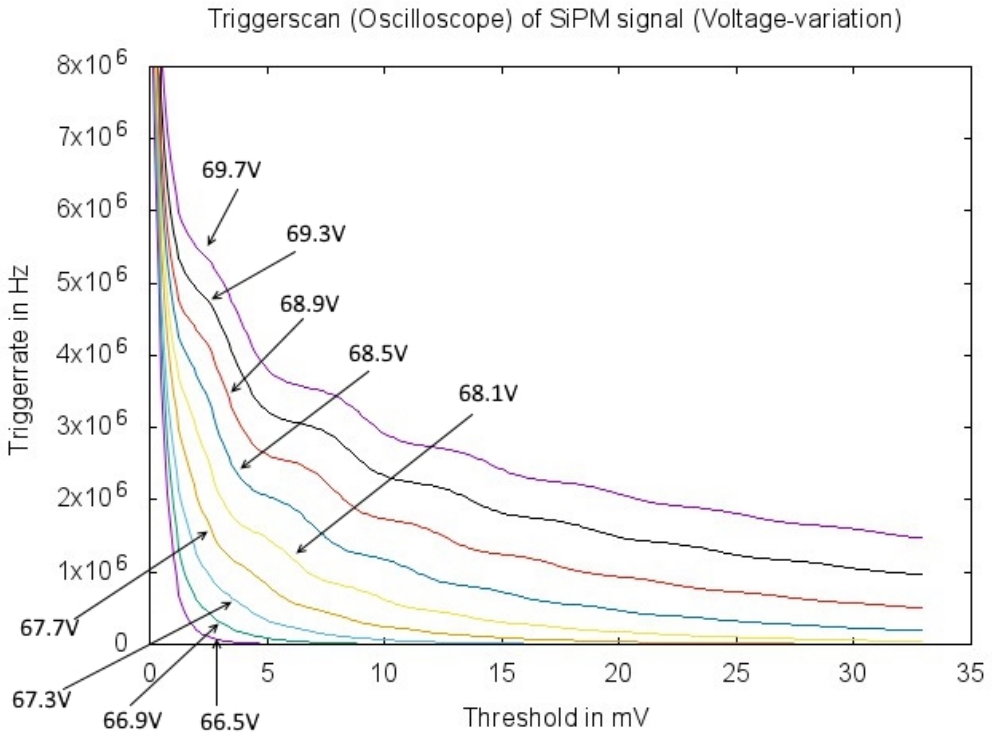

Figure 20: Triggerscan at different SiPM voltages

6.2 Measuring area of SiPM signal

Another method to determine the electrical charge is to measure the area of the waveform. In chapter 5.1 it was stated that the area of SiPM pulses is proportional to the number of p.e. that create the pulse. One advantage of this approach is that it is less biased by (high frequency-) noise because the noise is canceling out.
Again to get a first impression of how this area measurement on a SiPM looks like, an oscilloscope measurement was performed. Therefore, the horizontal range is set to 25 ns and the vertical range to 40 mV. Compared to Figure 15, it turned out that limiting the

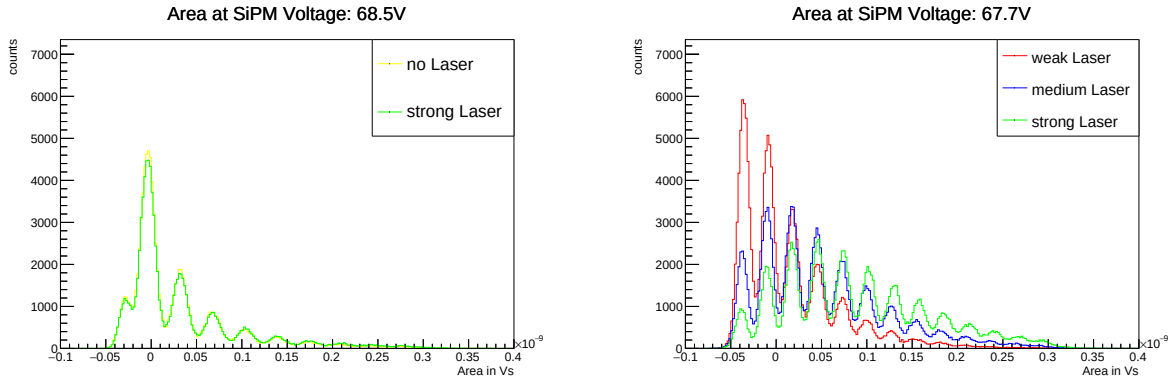

(a) Trigger on signal with 1 mV trigger threshold

(b) Trigger on laser pulse (5 kHz)

Figure 21: Influence of the laser luminosity on area

vertical range leads to more precise area determination even if the number of observable p.e. decreases to about 10. Since the TARGET ASIC is later also just calibrated to the first few p.e. (see chapter 7.2.2), a comparison is still possible.

6.2.1 Variation of laser intensity

The effect of the laser intensity on the area of the signal is tested hereafter. In Figure 21 one can see two area histograms. The left one shows results for triggering on the signal and the right one for triggering on the laser, each with different laser settings. All have in common that the pedestal[11] has a negative area because the baseline is at approximately $-1.5\,\mathrm{mV}$. In the left histogram there is only a minor difference between "no Laser" and "strong Laser" because the dark count rate of the Hamamatsu SiPM being used is rather large. Only the pedestal and first p.e. is a little weaker with laser because at a constant number of events that were measured, in this case 160000, the chance to get two or more p.e. slightly increases which leads to a decreasing of pedestal and one p.e.
This effect is a lot stronger in the right histogram. Triggering on the laser pulse means that the high dark count rate does not contribute much. Furthermore, the mean value of the distribution increases towards higher p.e. numbers if the laser intensity rises.
In appendix A.1 the laser dependency of the area is shown at different SiPM voltages (from 66.5 V to 68.9 V in 0.4 V steps) and both trigger options.

[11] first peak, events where no photon is detected

6.2.2 Variation of SiPM voltage

Similar to chapter 6.1.2 the influence of the SiPM voltage on the signal area was tested. The fact that the gain is growing with increasing voltage can be seen in both trigger options. But to explain the right plot another effect has to be taken into account because the distribution flattens out if the SiPM voltage increases. One can also say that low number p.e. (< 3) are replaced by high number p.e. ($\gtrsim 3$). This can be explained with crosstalk (see chapter 5.1).

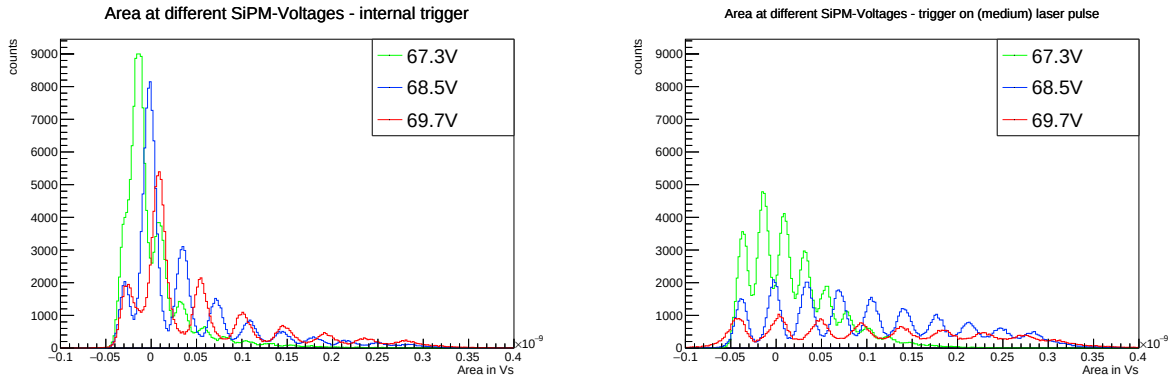

(a) Trigger on signal with 1 mV

(b) Trigger on laser pulse (5 kHz)

Figure 22: Influence of SiPM voltage on area

7 Performance of TARGET ASIC on SiPM

In the previous chapters several measurements with the reference oscilloscope on the SiPM were presented. In the following all the measurements will be adapted to the functionality of the TARGET ASIC. The Hamamatsu SiPM along with the buffer- and shaperboard provide an excellent opportunity to test TARGET under real conditions. The triggerpath of T5TEA can be examined by performing a triggerscan (see chapter 7.1.2), the datapath along with TC can be tested by doing area- (chapter 7.2.2) and amplitude scans (chapter 7.2.3). Furthermore, events can be taken and displayed combining trigger- and datapath (see chapter 7.2.1)
The trigger parameters that were used throughout all following measurements are listed in Table 1 in appendix A.2.

7.1 T5TEA

Testing the triggerpath of T5TEA with SiPMs provides helpful information of its trigger performance. Therefore, a triggerscan with the TARGET ASIC is done in the following chapter.

7.1.1 Calibration with PMTref4 - TRG_Thres scan

To perform a successful triggerscan with T5TEA the most vital parameters have to be adjusted. This is PMTref4 which is set for each trigger-group and controls the offset on the signal. On the other side it is TRG_Thres which controls the threshold itself (See 3.1). To compare this measurement to the one with the scope as reference (see Figure 26) a PMTref4-TRG_Thres scan has to be done in order to assign each parameter value pair to a threshold voltage (for more details see [11]).

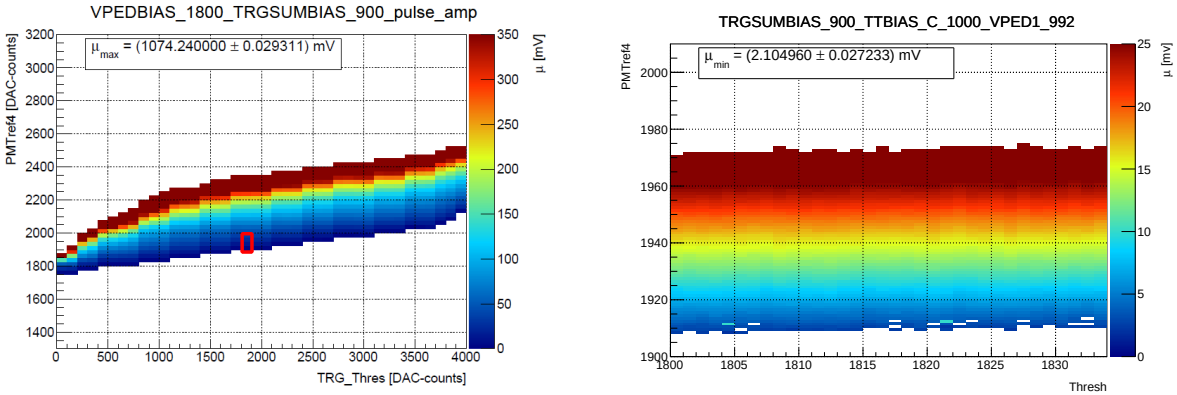

(a) Rough scan on wide range [11]

(b) More precise scan on narrow range

Figure 23: PMTRef4-TRG_Thres scan

Therefore, a small PMTRef4-TRG_Thres space was scanned with high precision i.e. 1 DAC stepsize (see Figure 23b). Since only threshold values up to 30 mV show significant p.e. peaks in the triggerscan (see Figure 20), the PMTRef4-TRG_Thres was only performed up to about 30 mV.

For the different Vped values settings (See Table 2,3) the result of the PMTRef4 - TRG_Thres scan is in appendix A.3.

7.1.2 Threshold measurement on SiPM signal

Since we have a translation of PMTref4 and TRG_Thres into threshold voltage, a triggerscan on a SiPM is possible. Figure 24b shows such a scan in 0.1 mV steps.
Since the PMTRef4 - TRG_Thres scan (see Figure 23b) is noisy (~ 0.4 mV, see errorplots in appendix A.3), the 0.1 mV step size leads to higher variation than the PMTref4 scan (Figure 24a) with ~ 1 mV step size.
The laservariation in Figure 25 shows the same behavior as seen in Figure 19.
In appendix A.4 the trigger- and PMTref4 scan is performed for various SiPM voltages. For the PMTref4 scan, the parameter TRG_Thres is set to 1820 DAC count. Figure 26 shows the comparison of T5TEA scan with oscilloscope triggerscan. Both curves are more or less identically. Even the first p.e. (~ 4 mV) can be resolved.

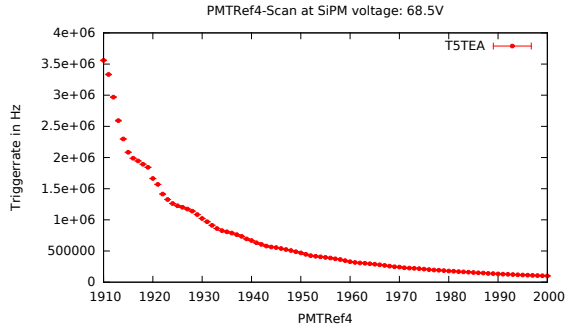

(a) PMTref4-scan

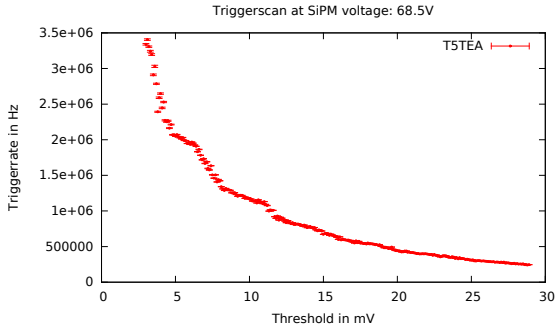

(b) converted threshold-scan (see Figure 23b)

Figure 24: T5TEA triggerscan on amplified and shaped SiPM signal

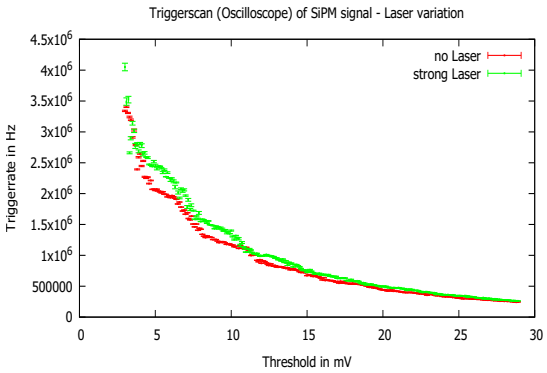

Figure 25: T5TEA Triggerscan with and without strong laser

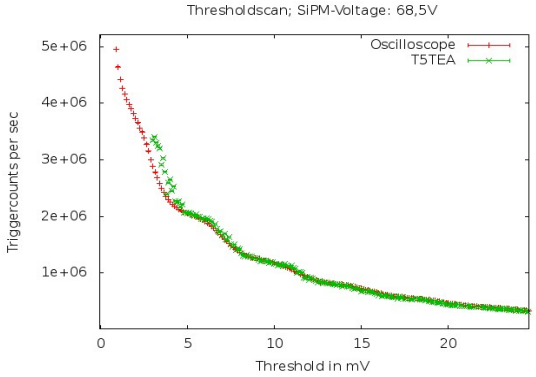

Figure 26: Comparison between TARGET and the oscilloscope

7.2 TARGET C

In the following chapter the datapath of the TARGET ASIC which refers to TARGET C is further tested. Since sampling does not work in channel 0 on the used evaluation board, the SiPM was connected to channel 1 throughout the whole measurements. Even if T5TEA and TARGET C are both used in the readout chain, the focus is on the datapath since triggering has already been tested in chapter 7.1.

7.2.1 Taking SiPM events without calibration

At the beginning, SiPM events were taken and displayed to get a first impression of how TARGET C behaves. Afterwards, a comparison with the oscilloscope measurement from chapter 5.2 can be done.

The following steps were performed:

- taking pedestal events
- taking SiPM events
- offset correction
- "common mode" correction

These steps are described in more detail hereafter.
At first, pedestal events are taken. Therefore, the SiPM voltage was lowered to 5 V to get the baseline without signal. The trigger for each event was set externally with the wave generator of the oscilloscope. The trigger frequency of 4 kHz meets the trigger dead time[12] which was set to 250 µs. This ensures that reading out the event is working properly [32]. For each pedestal event two storage blocks (64 samples) are read out. Then the exact position of every sample in the whole storage array, which consists of 512 blocks with 32 samples per block, is obtained. Therefore, the RowID[13] and ColID[14] is retrieved. With this information each block out of all 512 blocks can be addressed. Since the TARGET ASIC has a readout inaccuracy of 8 samples, which refers to a so called "Phase" the first sample of the waveform[15] does not need to start at the beginning of a storage block (but at multiples of 8 samples). By obtaining the offset ("Phase"), each sample of the read out waveform can be associated to a certain sample out of all 16384 samples of the storage array (with further information of RowID and ColID).
With this method one million pedestal events were taken. Then a mean pedestal value was calculated for each sample.

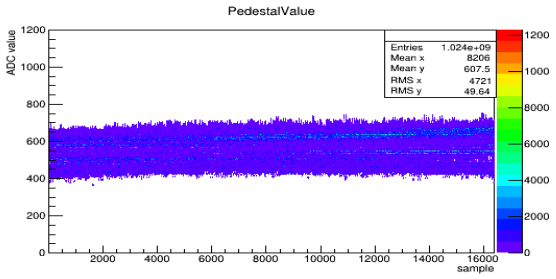

Figure 27: Pedestal value for each sample

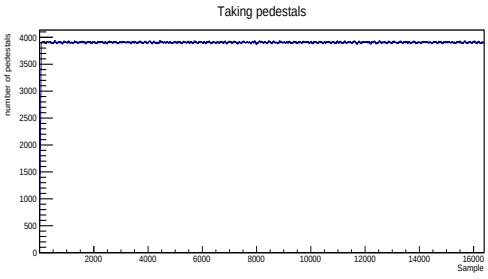

Figure 28: Number of pedestal events

[12] timerange after trigger in which no further trigger is accepted
[13] identifies the row of the storage array (from 0 to 7)
[14] identifies the column of the storage array (from 0 to 63)
[15] entirety of samples that are read out (here: 64)

Figure 28 shows the number of pedestal events per sample that ware used for calculation (3905 ± 9). One can see that the deviation is very small which means that the trigger method described above works properly. Figure 27 shows the pedestal value (in ADC counts) of every event.
After the pedestal events, SiPM events are taken in the same way. The only difference is the trigger behavior. Either one is triggering on the signal or on the laser pulse. In the first case the threshold voltage is set equally as in the threshold scan (chapter 7.1.2). In the other case the signal that controls the laser pulsing was connected to the external trigger connection of the evaluation board. The board itself was therefore set to "external trigger mode".
To compensate the delay between internal and external triggering, the trigger delay[16] of the FPGA was set to 440 DAC count for internal and 358 DAC count for external triggering. These values are obtained empirically and ensure that the signal peak is in the middle of the 64 read out samples (30 ± 4)[17]. Furthermore, the SiPM voltage is set to the desired value i.e. 68.5 V because here the gain has the expected value of $4 \frac{\mathrm{mV}}{\mathrm{p.e.}}$[19] (see chapter 8.2).

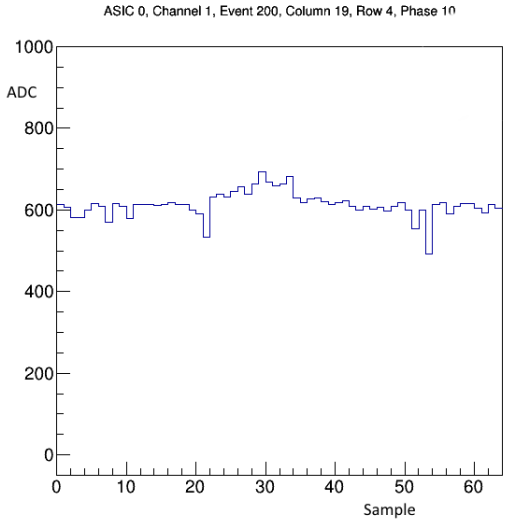

Figure 29: Example event without correction pedestal

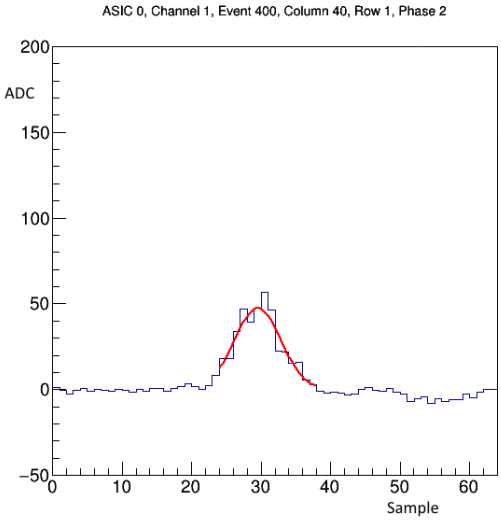

Figure 30: Example event after correcting pedestal

After taking real SiPM events the pedestal value for each sample is removed once the exact position of the sample in the whole storage array of TARGET C has been figured out. In Figure 29 one example event without pedestal correction is shown. In contrast to this the corrected event is shown in Figure 30.
One can see that the pedestal correction is essential to get a straight baseline which is

[16] shifts the events to read out with respect to the trigger point
[17] readout inaccuracy of 8 samples

shifted to zero. This is important if one wants to measure the area of the signal (see chapter 7.2.2) since baseline fluctuations could affect the result negatively.
The correction is also useful to compensate structural variations between the capacitors of the storage array. After subtracting the pedestal, another important correction is performed, the so called common mode correction. Therefore, the mean ADC value for each sample of channel 2-15 is removed from the same sample of channel 1 where the SiPM lays on. Since one expects that disturbances from outside the board (e.g. electromagnetic irradiation) affects all channel in the same way (common mode) they could be removed with this correction.
Since the exact position of each pulse is only known within 8 samples, a Gaussian functions is fitted to each pulse (see Figure 30). Since the horizontal position of the pulse can be obtained from the fit, it is possible to put all events on top of each other. This yields the plot from Figure 31 (5 mV threshold) and 32 (trigger on laser pulse). Analogous to the oscilloscope image in chapter 5 the baseline is present at triggering on laser pulse. At 5 mV threshold voltage, the baseline is cut out. Due to noise T5TEA still triggers on some 1 p.e. events with ≈ 4 mV.
In general one can say that it is much more difficult to see each p.e. on TARGET ASIC than on the oscilloscope. The reason for this is on one hand the 4 times larger sample rate of the used oscilloscope (4 GSa/s). This leads to a 4 times higher amount of sample values for the same SiPM signal and thus leads to a more accurate digitalization. More important, however, is the fact that the 12 bit digitization of signals with a high voltage range up to 2.5 V is much more inaccurate than 8 bit digitization of the oscilloscope that has a variable vertical (voltage) window [21]. In TARGET C one digital ADC unit corresponds to ≈ 1 mV while at the scope one digital unit corresponds to $\frac{256}{40} \approx 0.16$ mV at the used vertical range (see chapter 5.2). In addition to this, the noise of the oscilloscope is smaller (0.16 mV-0.24 mV) than the noise of the TARGET C (0.6 mV-1 mV). At last, the samples of the oscilloscope does not need to be calibrated, unlike the the storage array of TARGET C (see next chapter) [32].

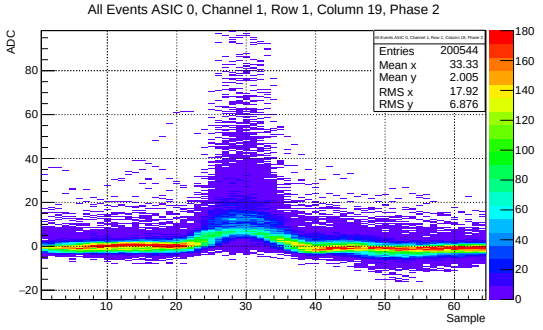

Figure 31: Multiple amplified and shaped SiPM events with internal trigger (5 mV)

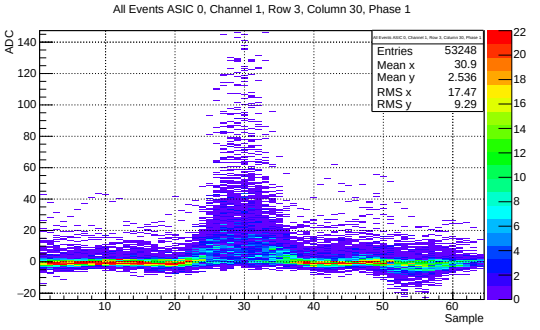

Figure 32: Multiple amplified and shaped SiPM events with trigger on laser pulse

7.2.2 Area calibration of TARGET C

Now one wants to calculate the area of each signal after the above corrections were performed. As in the oscilloscope measurement in chapter 6.2, the area gives a rather good possibility to obtain the number of photons (p.e.) that made the event.
To obtain the area of the corrected signal (see Figure 30) one has to find the peak at first. Therefore, the sample with highest ADC counts (MaxBin) was obtained in a range 6 samples around 30th sample (see Figure 30). The limited "search window" ensures that noise does not sophisticate the result due to the fact that noise is mostly located outside the window especially if one is triggering on laser pulse. Next step is a Gaussian fit around ($\pm$7 samples) "MaxBin" . Then ADC values are added together from "FitMean" -10th to "FitMean" +10th sample where "FitMean" is the obtained mean value of the fit, the exact position of the peak. The 20 ns time range, in which the area is calculated eventually, covers the whole signal (see Figure 30).
Figure 33 shows a histogram of the thus calculated area (in ADC). The threshold voltage is set to 5 mV. First of all, one can see a plateau at around zero area together with negative

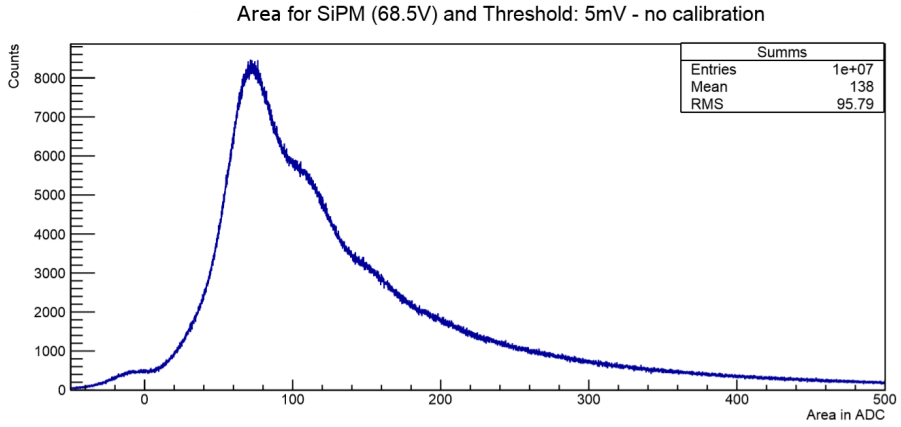

Figure 33: Area measurement of SiPM signal without calibration

area values. This comes from some events where the triggering was one clock cycle (8 samples) to late. Since the waveform is then outside the "search window". The area is then calculated from the baseline which fluctuates around zero ADC [32]. Furthermore, it becomes obvious that, apart from the second p.e., which correspond to ~ 8 mV no other peaks are visible. This is mainly because of structural variations between the capacitors of the storage array. The obtained area hence depends on the storage block the signal is "written".
Therefore, an area calibration has to be done. In this calibration, signals with known amplitude are read out (see chapter 5.2). Then the exact sample position in the storage block and the area (in ADC) is obtained. Figure 34 shows the measured area for a 40 mV signal as a dependency of the sample in which the signal "falls".

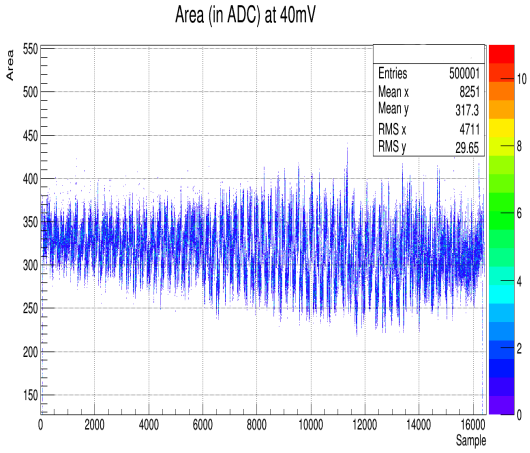

Figure 34: Area calibration for 40 mV signal

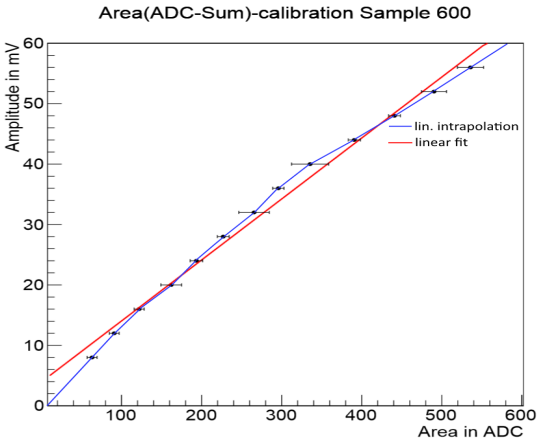

Figure 35: Calibration result for one sample with linear fit (red) and linear interpolation (blue)

This calibration was performed for different signal amplitudes (from 8 mV to 156 mV in 4 mV steps). Figure 36 and 37 show the measured area, averaged over all samples, as a function of the signal amplitude. Both plots have two different Vped settings (see Table 2 and 3) and have different shape, especially at lower amplitudes. This correlates with the so called transferfunction which shows the ADC count of one sample as a function of the input voltage. The so called linear range is then the range where both entities have a linear dependency of each other [19]. Increasing the Vped value for all 16 channels leads to a rising input voltage and thus leads to extended linear range for smaller amplitudes. In all following measurement all 16 Vpeds are therefore set to 1100 DAC counts.
For each sample a linear fit has been made (see Figure 35). With this fit each area ADC-value can be referred to a amplitude with which the number of p.e. can be determined.

Since the focus is to display the first few p.e., a second area calibration has been performed (ranging from from 8 mV to 56 mV in 4 mV steps) as one can see in Figure 38. In this plot the measured mean area and deviation (color), respectively, is shown for all used amplitudes and samples. First to mention is the small deviation compared to Figure 34. The fact, that area determination within one sample is much better than the determination over all 16384 sample, shows that a calibration of the storage array is essential.

To further test the calibration, pulses with known amplitude were read out. The amplitude was measured with the area calibration as seen above. Figure 39 shows the result. There is still high deviation (3.9 mV at 40 mV). Furthermore, there is a special pattern with ~ 256 sample periodicity which probably comes from the 8 blocks column pattern.

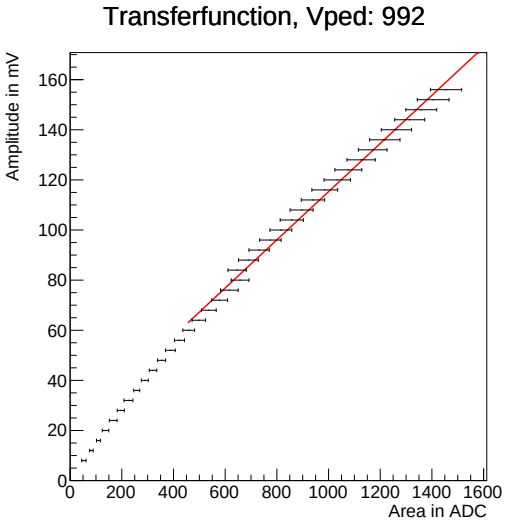

Figure 36: Transferfunction for VPED 992

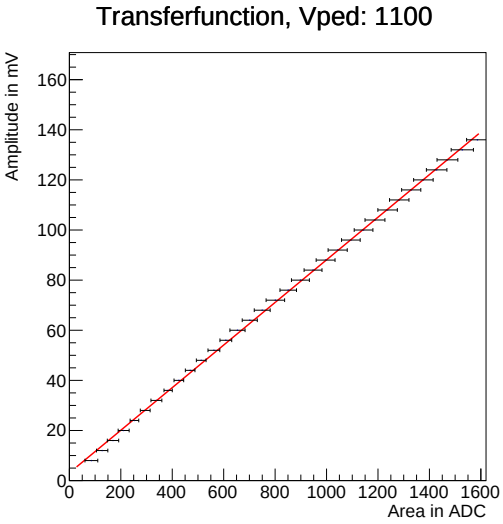

Figure 37: Transferfunction for VPED 1100

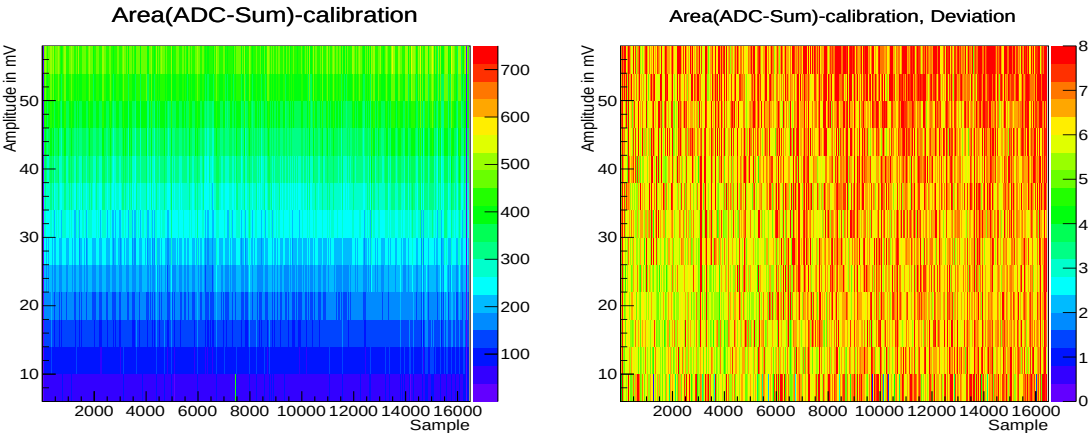

Figure 38: Complete result of the calibration for all 16384 samples

To solve this problem, the linear fit was replaced by a linear interpolation[18] for amplitudes ranging from 8 mV to 56 mV and linear extrapolation[19] for other amplitude values. The example fit for sample 600 from Figure 35 shows the advantage of inter(extra-)polation over the linear Fit. In contrast to the linearity of Figure 37, one sample shows no linear behavior (see Figure 35).

[18] Linear connection between two adjacent calibration measuring points[33]
[19] Creating a tangent line at the end of known data and extending it beyond that limit[34]

The new interpolation method actually improved the result (see Figure 40). The deviation decreased to 2.7 mV at 40 mV. Compared to the uncalibrated measurement (30 ADC deviation at 317 ADC, see Figure 34) the relative error (derivation divided by mean value) improved from 9.5% to 6.8%.
Since there is still a 8 blocks column pattern (256 samples periodicity) in Figure 40, further studies and stability tests have to be performed.

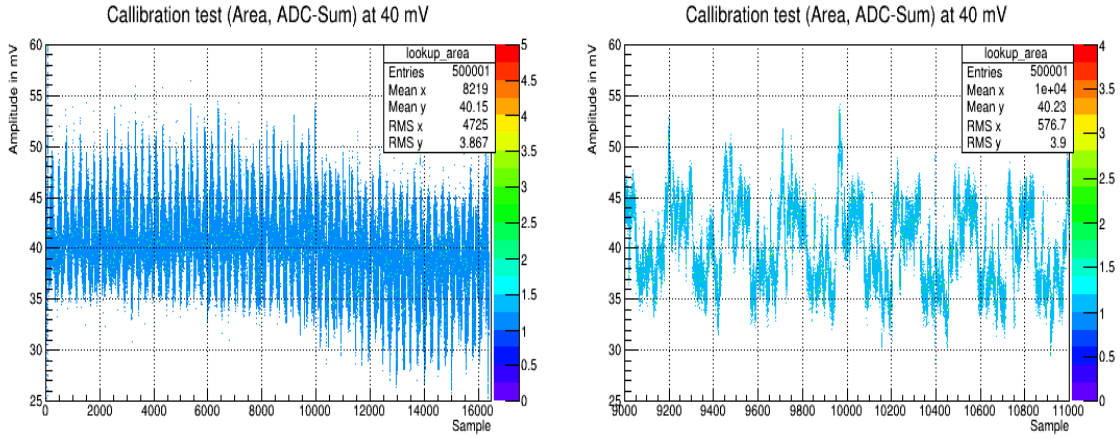

Figure 39: Testing area calibration (linear fit) with 40 mV signal for all samples in the storage array (left) and zoomed in (right)

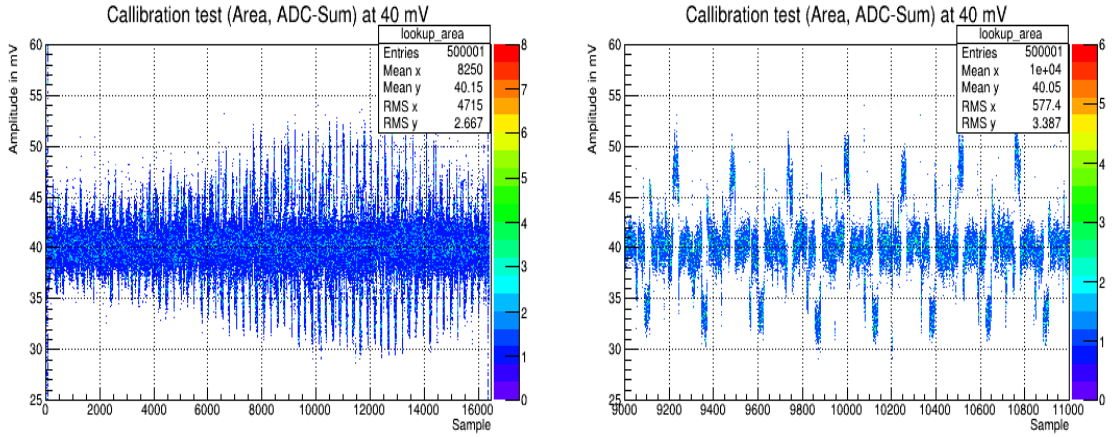

Figure 40: Testing area calibration (interpolation) with 40 mV signal for all samples in the storage array (left) and zoomed in (right)

The calibration was performed with the modeled pulse and the standard pulse (see Figure 7.2.2 in chapter 5.2). The overall aim is to model the real SiPM signal as good as it is possible. Otherwise the conversion from area (in ADC) to amplitude is failing. That is because the area of the modeled signal and the SiPM signal is different at the same

amplitude.
Figure 41 shows the same calibrated area measurement on SiPM signal, but with different calibration pulse shapes, both with 5 mV threshold voltage. In the left plot the calibration was done with the modeled waveform and the calibration for the right plot was performed with a "standard" pulse. One can see that the modeled waveform yields the best results since here the peaks are at multiples of 4 mV. Since the standard pulse has a larger area (see Figure), the peaks were shifted to lower amplitudes (see 5. p.e. which should be at ~ 20 mV).
Furthermore, following things are to mention: the counts around 4 mV occur due to fit problems. The lowest signal amplitude at calibration was 8 mV which leads to high extrapolation uncertainties for small amplitudes. The rise at around 5 mV is a "real" effect that originates from noise on the triggering.

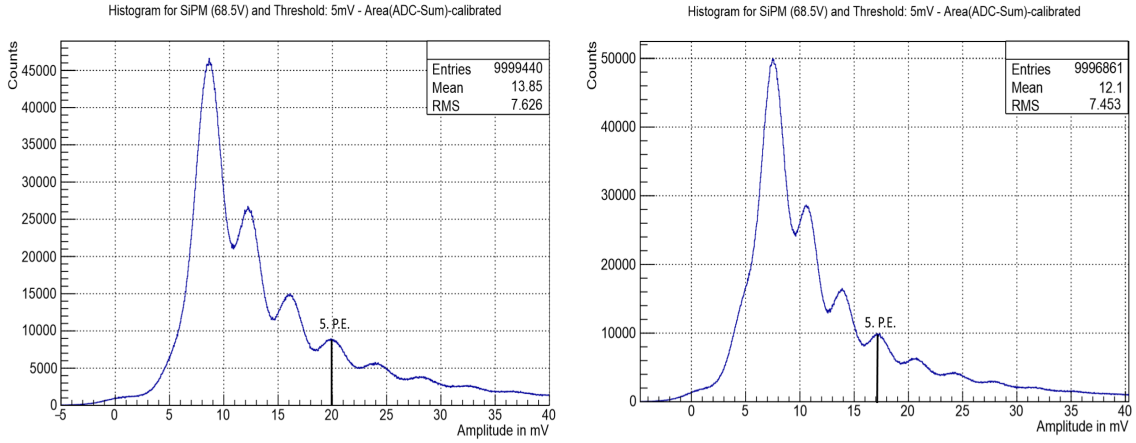

Figure 41: Calibrated area measurement (5 mV threshold) on amplified and shaped SiPM signal with modeled waveform (left) and standard pulse (right)

Furthermore, an area measurement was performed while triggering on the laser signal. Figure 42 shows the result. One can see that the calibration, in this case with interpolation, does not improve the results much (only at higher p.e.). This shows that the equality of the storage capacitors is given for small amplitudes. Additionally there is a again no pedestal (see fit problem above). The uncalibrated measurement is better than the one with internal trigger at 5 mV threshold because there is less noise. That is because noise with e.g. more than 5 mV is triggered on with the internal trigger but not necessarily with triggering on laser pulses.
In appendix A.5 the area measurement on SiPM is performed at various SiPM voltages all with internal trigger and trigger on laser pulse.

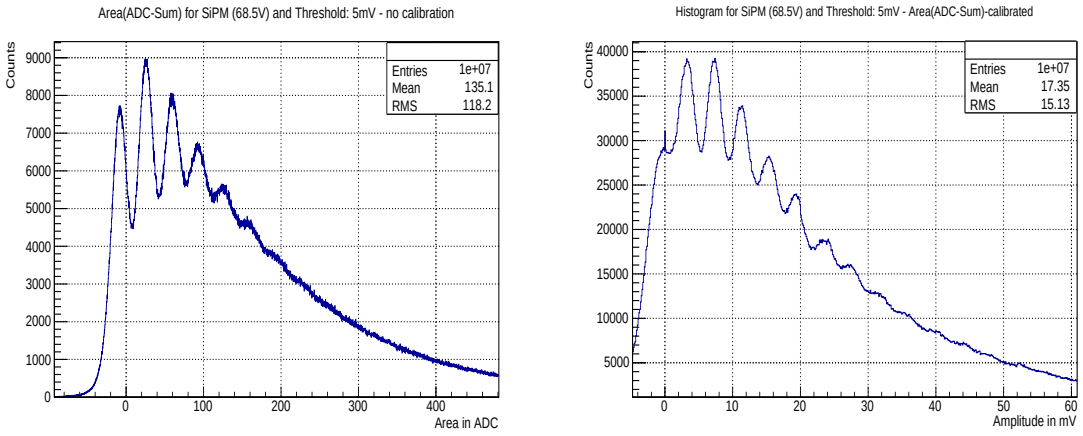

Figure 42: Area measurement (trigger on laser pulse) on amplified and shaped SiPM signal with (right) and without (left) calibration

7.2.3 Amplitude calibration of TARGET C

In this chapter an amplitude calibration is performed. The only difference to the area measurement that was performed in the previous chapter is that the amplitude is determined by finding the largest ADC value in the "search window". Figure 43 shows this measurement on amplified and shaped SiPM signal. It is not possible to see any p.e.-Peak apart from the 2. p.e. with 8 mV. Even if the amplitude is determined via Gaussian fit as seen in Figure 44, one can see hardly any p.e. events.
The reason for this is the high sensitivity to noise. One short noise peak e.g. could be misinterpreted as a SiPM event. Furthermore, there is the sampling rate to mention (1 GSa/s). At such short events (~ 15 ns) there are only a few crucial samples. The sample with the highest ADC value is, however, not at the exact peak position in most cases. That is why the digitization process itself limits the amplitude resolution and therefore an area measurement (see previous chapter) is a rather better method.

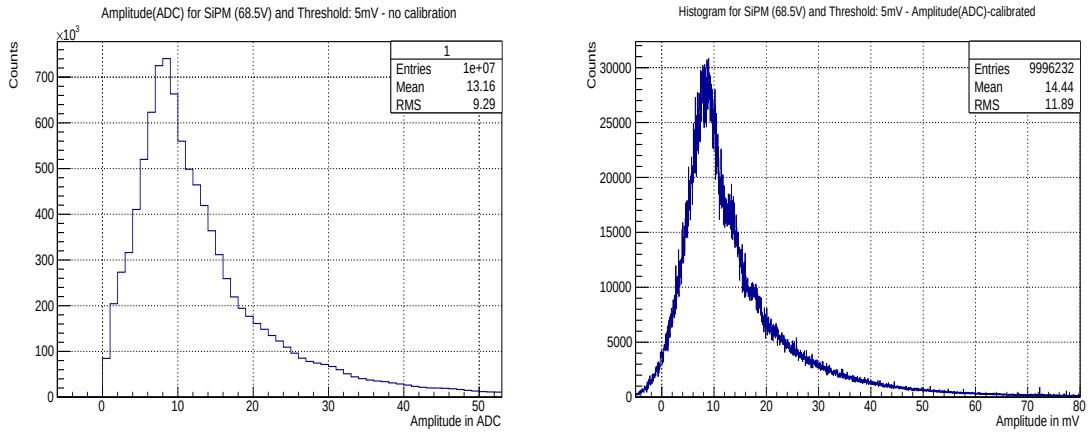

Figure 43: Amplitude measurement on SiPM with (right) and without (left) calibration

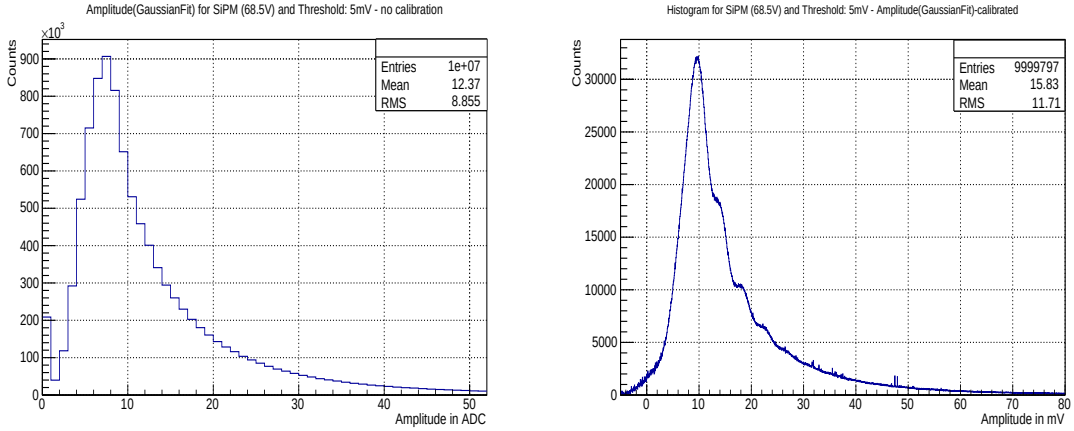

Figure 44: Amplitude measurement (Gaussian Fit) on SiPM with (right) and without (left) calibration

8 Comparison of TARGET ASIC with reference oscilloscope

In this section, the TARGET measurement is compared to the oscilloscope measurement that was performed previously. Furthermore, important electrical quantities of the used SiPM like gain or crosstalk are determined.

8.1 Charge resolution

The charge resolution gives useful information of how good events with different photon number can be distinguished. Since the area of the SiPM signal is proportional to the number of photon events, the area measurement is used to calculate the charge resolution.

Therefore, single Gaussian functions are fitted to each p.e.-peak (see Figure 61 in appendix A.6). The relative charge resolution Q is than defined as the σ value of the Gaussian fit divided by the position.
Figure 45 shows a comparison of charge resolution, calculated for different TARGET measurements and a comparison to oscilloscope measurement (see Figure 61). One can see that the area measurement with internal trigger and calibration shows the best results even if the oscilloscope has a resolution which is approximately three times better. It should be noted that this charge resolution was measured only with the amplified and shaped SiPM signal. Under real conditions, other technical (crosstalk, quantum efficiency[20]) and physical effects (NSB[21], Poisson noise[22]) further worsen this charge resolution. [32]
The NSB ($\sim 125\,\mathrm{kHz}$) and the Poisson noise are the only quantities that can be estimated in the scope of this thesis . With this consideration, the obtained relative charge resolution is 0.416 for the second p.e. and 0.212 for the 8th p.e. which is still better than CTA requirements which can be seen in Figure 46 (~ 1 for 2nd and ~ 0.4 for 8th p.e., respectively).
The charge resolution was obtained with the following formula [32].

$$\frac{\Delta Q}{Q} = \frac{1}{Q}\sqrt{Q + \mathrm{NSB} + \mathrm{noise}^2}$$

$\frac{\Delta Q}{Q}$ is the relative charge resolution, Q the position of the p.e.-peak, noise the σ value of the Gaussian fit and NSB the rate of background photons within the 20 ns window where the area is determined.

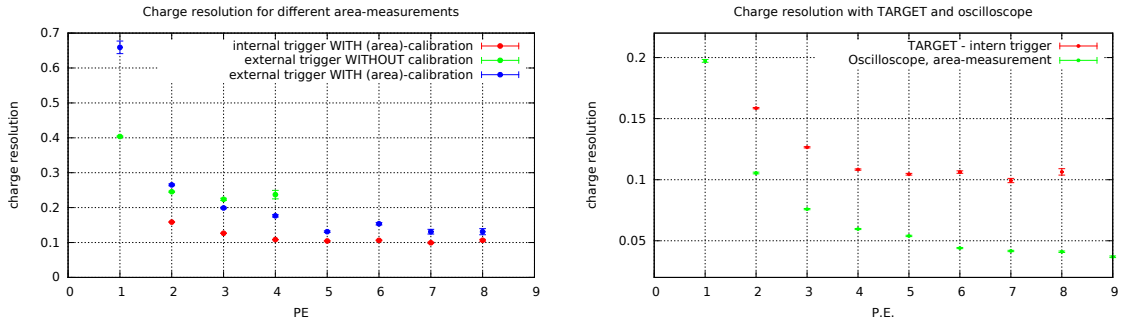

Figure 45: Charge resolution for various TARGET measurements (left) and compared to oscilloscope measurement (right)

One has to mention that these obtained values are still underestimated because the single Gaussian fit is always influenced by adjacent photon events. For exact values, a multi Gaussian fit has to be performed.

[20] Probability that an incoming photon induces a photoelectron[23]
[21] **N**ight **s**ky **b**ackground
[22] Photon number of physical identical Cherenkov flashes follow Poisson distribution

Summing up, one can say that the charge resolution, determined in this thesis, are only a first estimation. Further analysis has to be done, considering the above mentioned aspects.

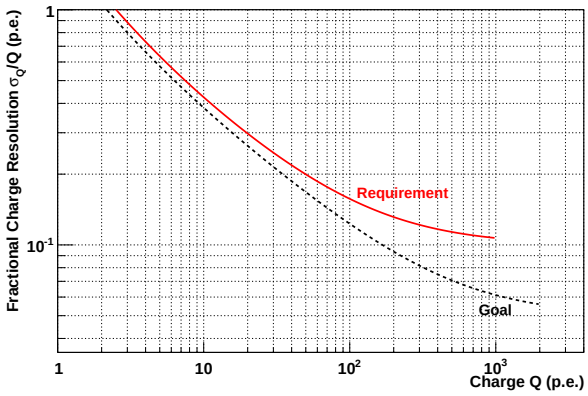

Figure 46: CTA requirements for charge resolution[9]

8.2 Gain

The gain of the SiPM gives information about how the amplitude of the signal increases with increasing p.e. number. Here the triggerscan as performed in chapter 6.1 and 7.1.2 was used. Since the slope of the curve has its lowest value while the threshold voltage passes over the p.e. waveform, the derivative was used. The exact position of the p.e. was determined via Gaussian fit. The gain was afterwards calculated as the amplitude difference between second and third p.e. as one can see in the oscilloscope triggerscan in Figure 47.

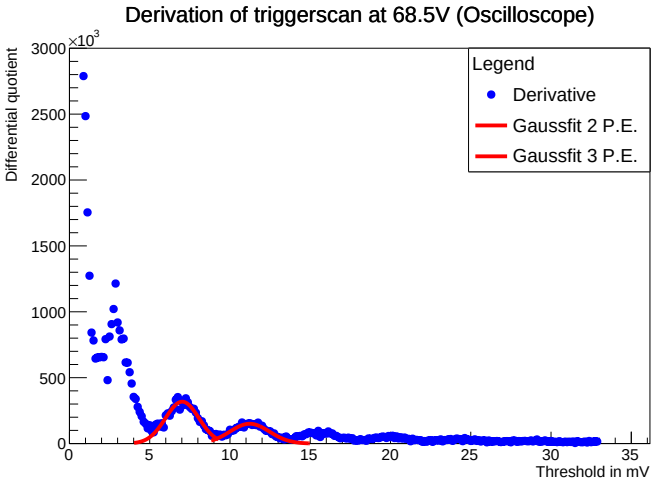

Figure 47: Determination of gain using the triggerscan

Figure 48 shows the calculated gain at different SiPM voltages. T5TEA is able to determine the gain even if the errors are larger due to noise in the triggerpath. Since the PMTref4-scan shown in Figure 24a is smoother, the gain can be determined even better, after each PMTref4 was converted into a threshold voltage (see chapter 7.1.1).
Figure 62 in appendix A.7 shows the derivative of the triggerscan for various SiPM voltages.

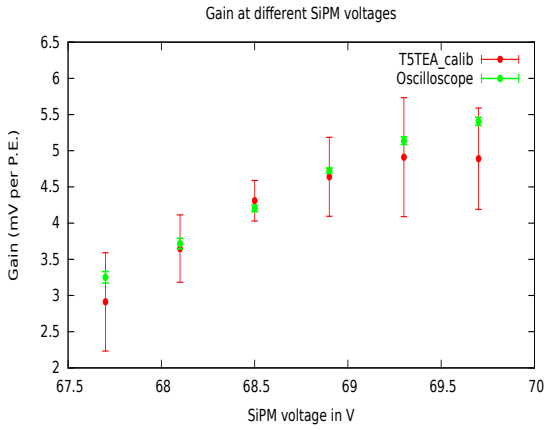

Figure 48: Gain at different SiPM voltages

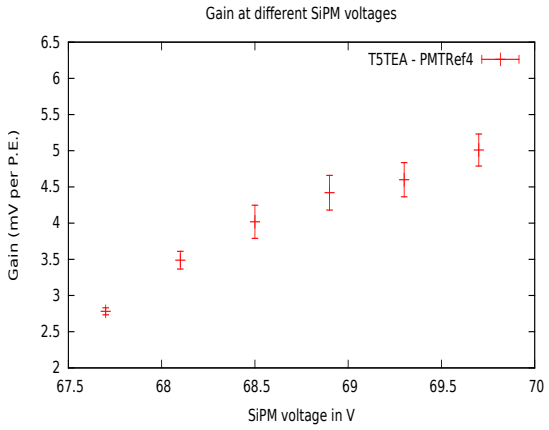

Figure 49: Gain at different SiPM voltages from T5TEA PMTref4-scan (see Figure 24a)

8.3 Crosstalk

As stated in chapter 5.1, crosstalk is a negative effect that sophisticates the photon counting process. To estimate the crosstalk, a Poisson distribution was fitted to the area spectrum. In Figure 50 the crosstalk is determined with oscilloscope (see 6.2) and TARGET (see 7.2.2). Since the pedestal is essential for an adequate fit, the measurement with trigger on laser and without calibration was used for TARGET. The red dashed line shows the expected p.e. peak if one assumes no crosstalk. "1ph+ crosstalk" is the probability that at least one crosstalk-photon is detected. If at least one crosstalk-photon was detected, "2ph+ crosstalk" gives the probability that two (or more) crosstalk-photons are detected and so on.
Furthermore, one can see that the fit for TARGET measurement has not worked properly. This comes from the fact that the pedestal peak is to broad due to baseline fluctuations and TARGET noise. Since the fit program is originally designed for PMTs which have a narrow pedestal, further investigations have to be done in order to adapt the program to SiPMs and TARGET [32]. Furthermore, the charge resolution (see 8.1) can be determined more accurately if the crosstalk is known.

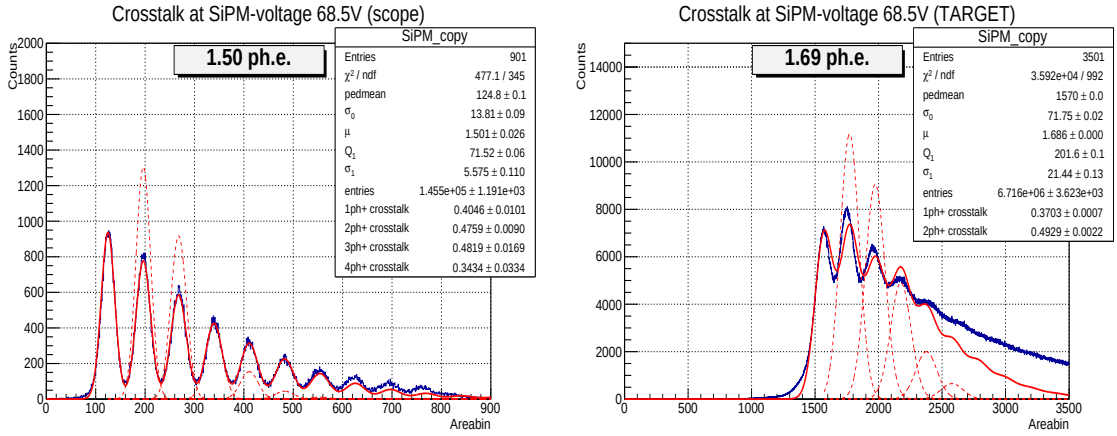

Figure 50: Crosstalk determination with oscilloscope (left) and TARGET (right)

9 Conclusion

Many different measurement with the amplified and shaped SiPM signal have been performed. At first, it was shown how the signal behaves with changing bias voltage and laser intensity. Oscilloscope images visualized variations of gain and undesirable effects like the high dark count rate. Furthermore, the geometry of the signal was analyzed. The FWHM is 9.3 ns, the leading and falling edge is 5.6 ns and 7.0 ns, respectively. With this, the SiPM signal could be modeled with the wave generator which is useful for calibration of TARGET C storage array. To test the trigger performance of T5TEA, a triggerscan on the SiPM signal has been performed. It turned out that this triggerscan is almost identical to the reference oscilloscope measurement. This shows that T5TEA has a good trigger performance. Even on one p.e. signals with ~ 4 mV, triggering is possible. With the help of the triggerscan, the gain was calculated. To determine the number of photons that lead to a particular SiPM pulse, the area of each pulse was determined in a 20 ns range around the peak. It turned out that this method leads to a better result than measuring the pulse amplitude because it is less affected by noise. Furthermore, it has been shown that a calibration of all 16,384 capacitors of the storage array is essential. The transferfunction is not linear, especially for low amplitudes. Therefore, extrapolating the measured area for each sample yields better results. With this calibration, the area of a 40 mV pulse can be determined with a relative error of 6.8% compared to the 9.5% error without calibration. First estimations of charge resolution with consideration of NSB and Poisson noise give a improvement of CTA requirements by a factor of two for the first eight photoelectrons.

10 Outlook

It has been shown that a calibration of the TARGET C storage array improves the charge resolution. Nevertheless, the calibration process has to be investigated further since the measured area still depends on the sample of the storage array in which the waveform was buffered. Furthermore, the calibration can be extended to amplitudes $> 60\,\mathrm{mV}$. But also the sampling of pulses with amplitudes $< 8\,\mathrm{mV}$ is of high astronomical importance in order to detect faintest Cherenkov flashes. Additionally, the programming script that performs multi Gaussian fit and thus determines crosstalk has to be further investigated in order to fit the peaks of the TARGET area measurement correctly. Since the read out was only performed with channel 1, the calibration of the TARGET C storage array can also be done on the other 15 channels. Finally, testing the TARGET ASIC on the whole camera that has SiPMs as photosensors is of great importance. This is likely to be realized in this year with the CHEC-S camera that is used in GCT[16].

A Appendix

A.1 Areascan at different laser intensities

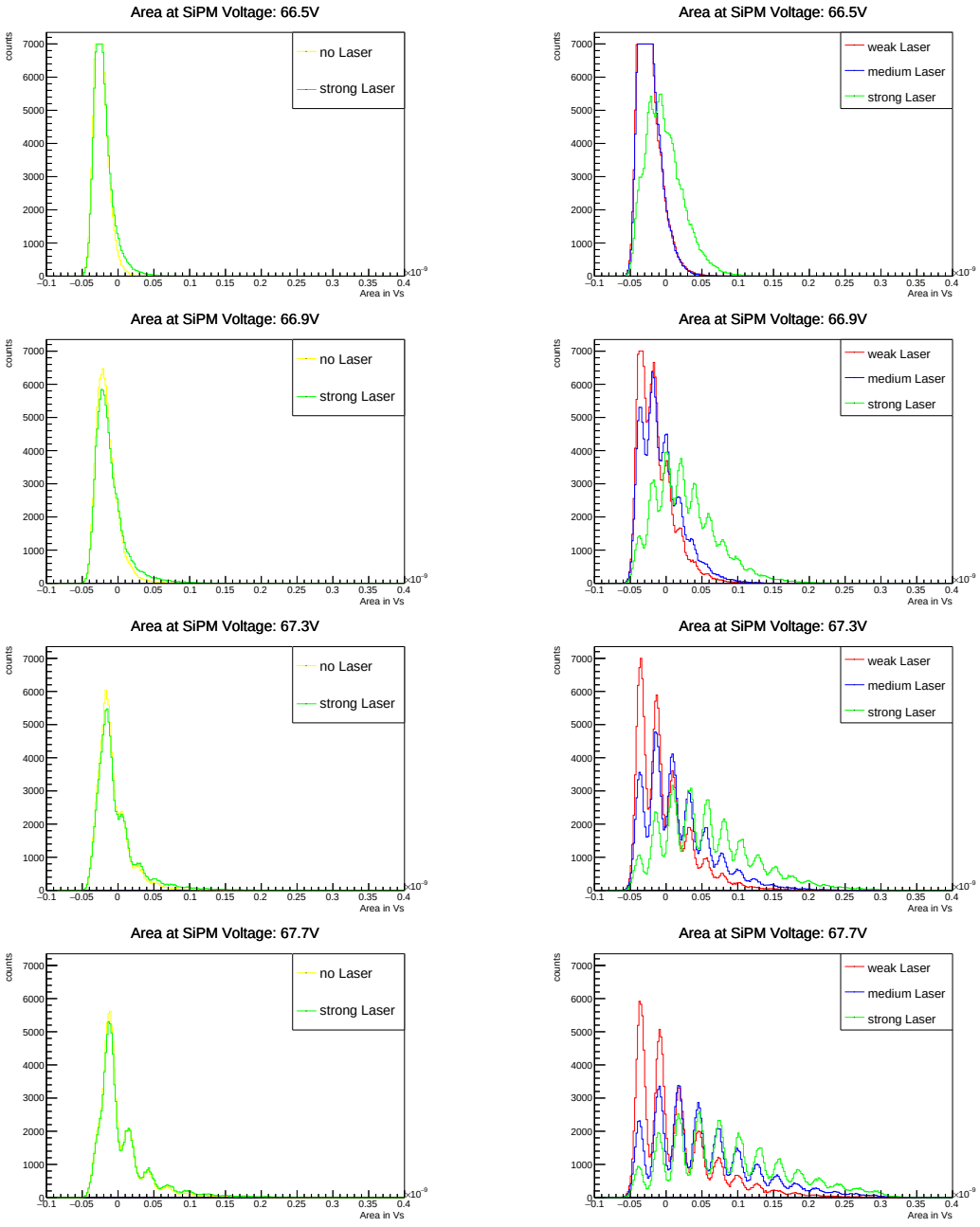

Figure 51: Dependency of signal area and laser intensity (oscilloscope) with 0 mV threshold (left) and trigger on laser pulse (right)

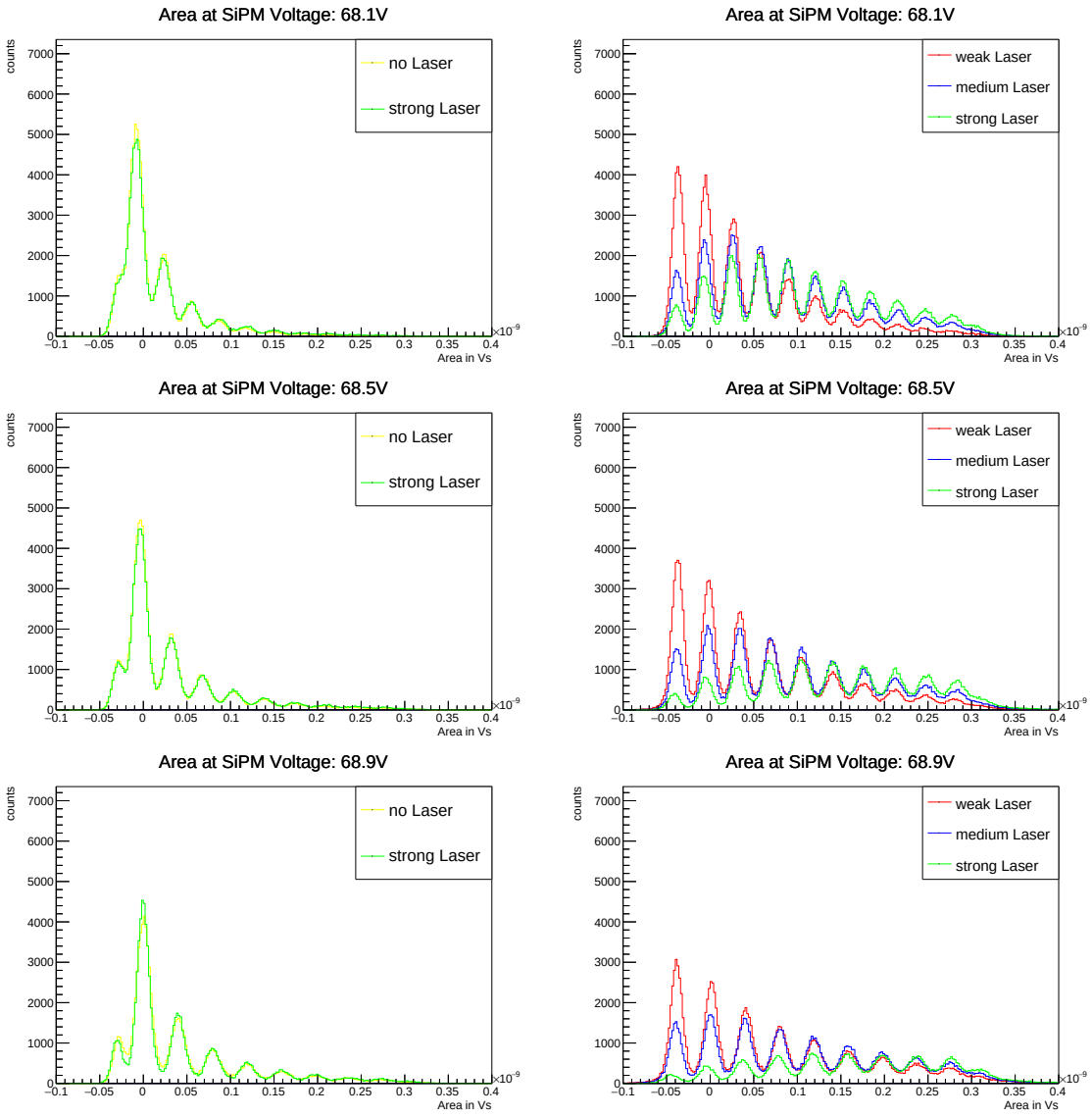

Figure 52: Dependency of signal area and laser intensity (oscilloscope) with 0 mV threshold (left) and trigger on laser pulse (right)

A.2 Default values (T5TEA)

In all measurements made with the whole TARGET ASIC the following parameter values for the triggerpath of T5TEA are used [20]. It was figured out that lowering TRGsumbias from 2400 to 900 improves the trigger performance of T5TEA by lowering the noise.[11]

Parameter	Value [DAC–counts]
VpedBias	1800
TRGsumbias	900
TRGbias	1000
TRGGbias	1900
TTbias_0	1100
TTbias_C	1000
TTbias_A	400

Table 1: Default values

Furthermore there were two different Vped settings used. In the first one all 16 Vped were set around DAC value 1000, apart from the first triggergroup, were variations in the signal offset for each channel were compensated.

Parameter	Value [DAC–counts]
Vped_0	1000
Vped_1	992
Vped_2	1005
Vped_3	998
Vped_4 ... Vped_15	1000

Table 2: First additional Vped setting

In the second Vped setting all Vped DAC values for each channels were set to 1100

Parameter	Value [DAC–counts]
Vped_0 ... Vped_15	1100

Table 3: Second additional Vped setting

A.3 PMTRef4 - TRG_Thres scan

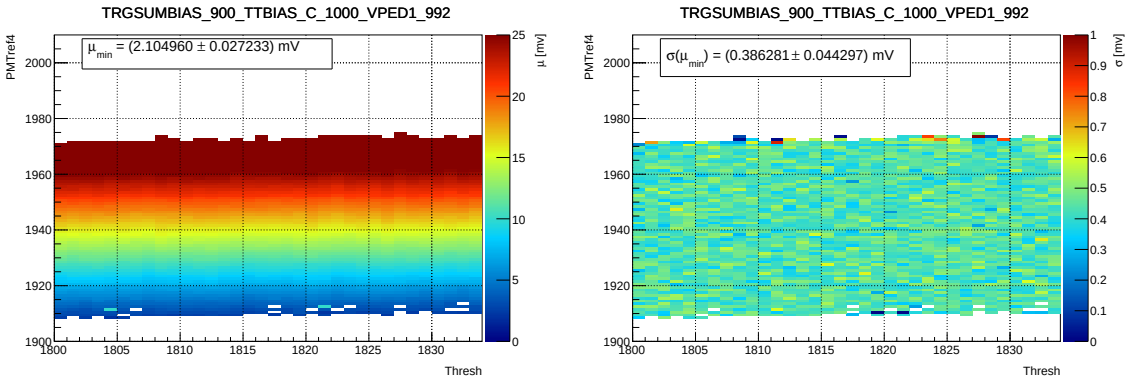

Figure 53: PMTref4 - TRG_Thres scan with Vped 1000 (See Table 2)

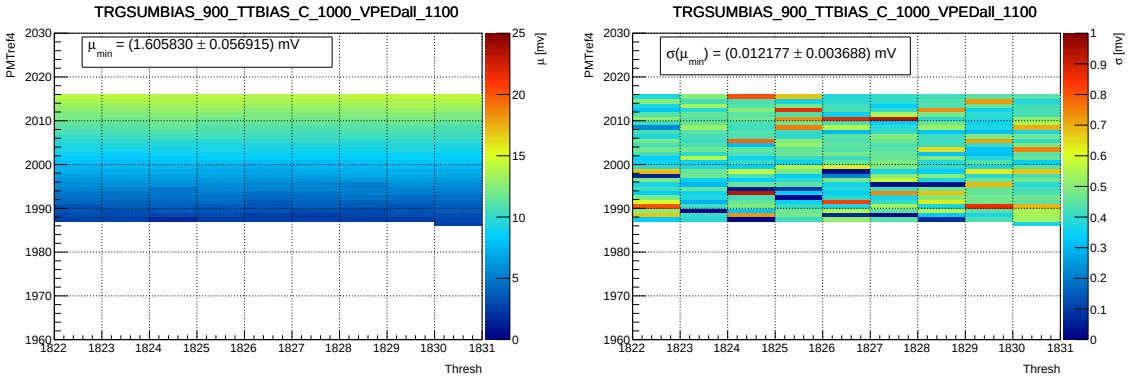

Figure 54: PMTref4 - TRG_Thres scan with all Vped 1100 (See Table 3)

A.4 T5TEA triggerscan on SiPM

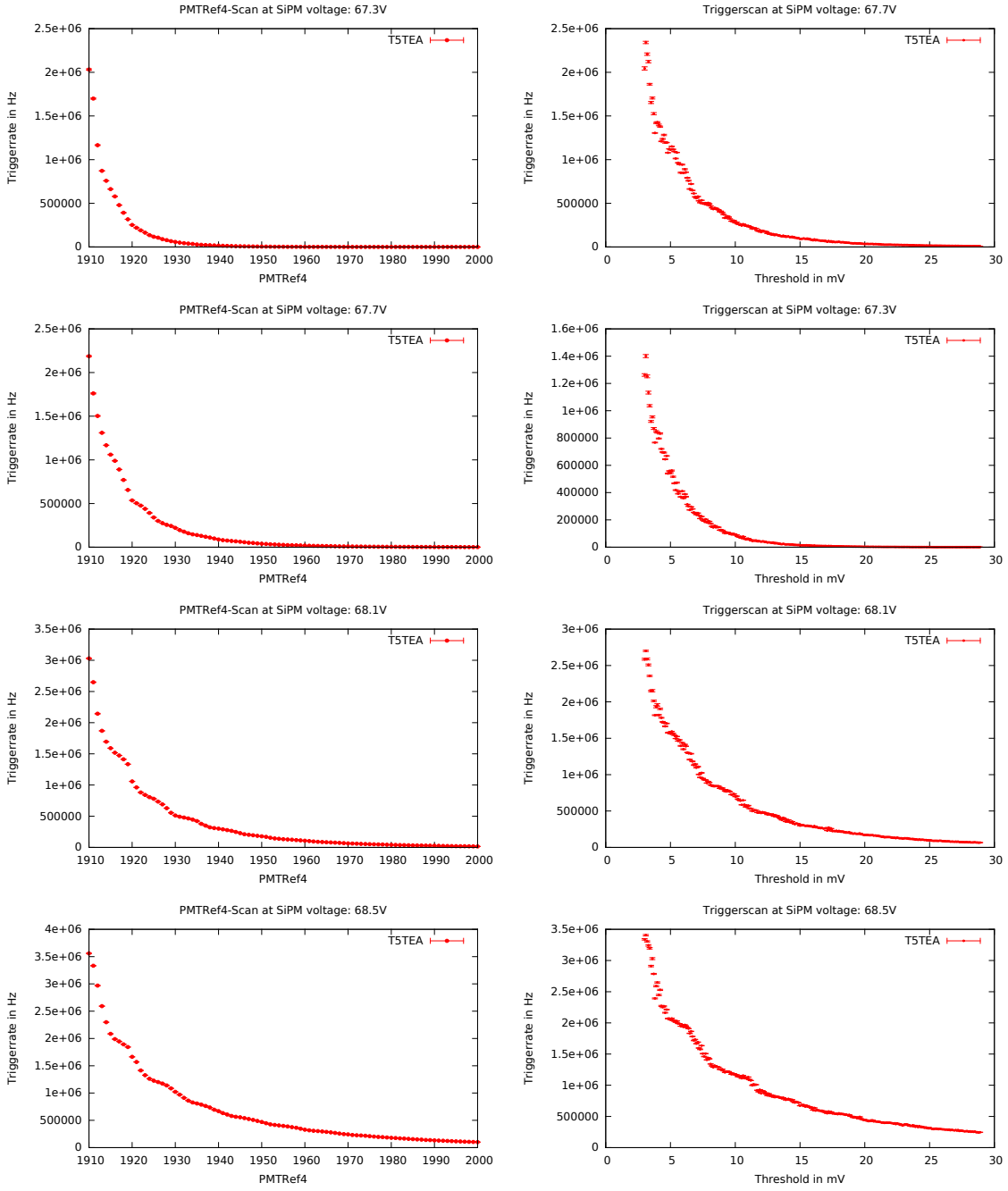

Figure 55: PMTref4-Scan (left) and converted threshold-scan (right) for different SiPM voltages

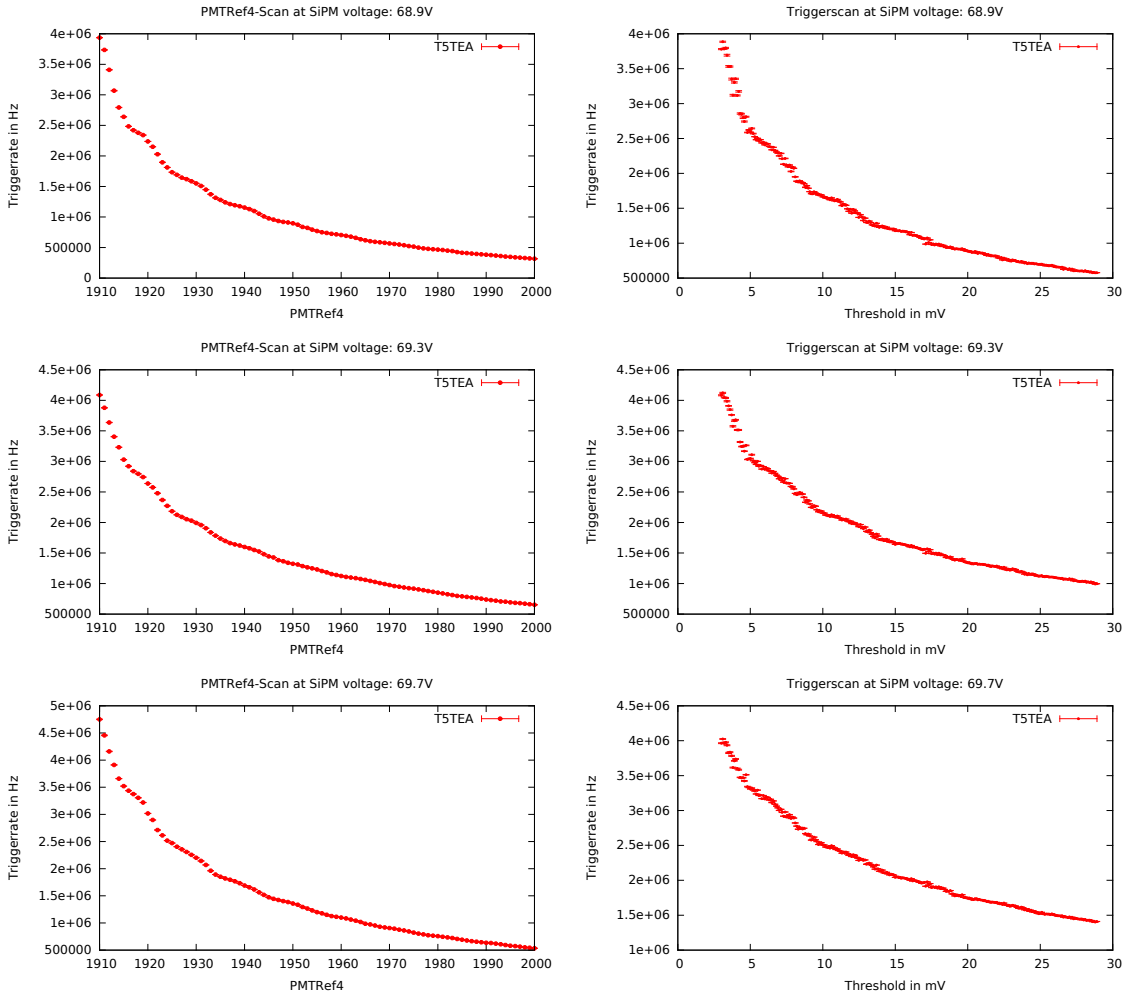

Figure 56: PMTref4-Scan (left) and converted threshold-scan (right) for different SiPM voltages

A.5 calibration of TARGET C

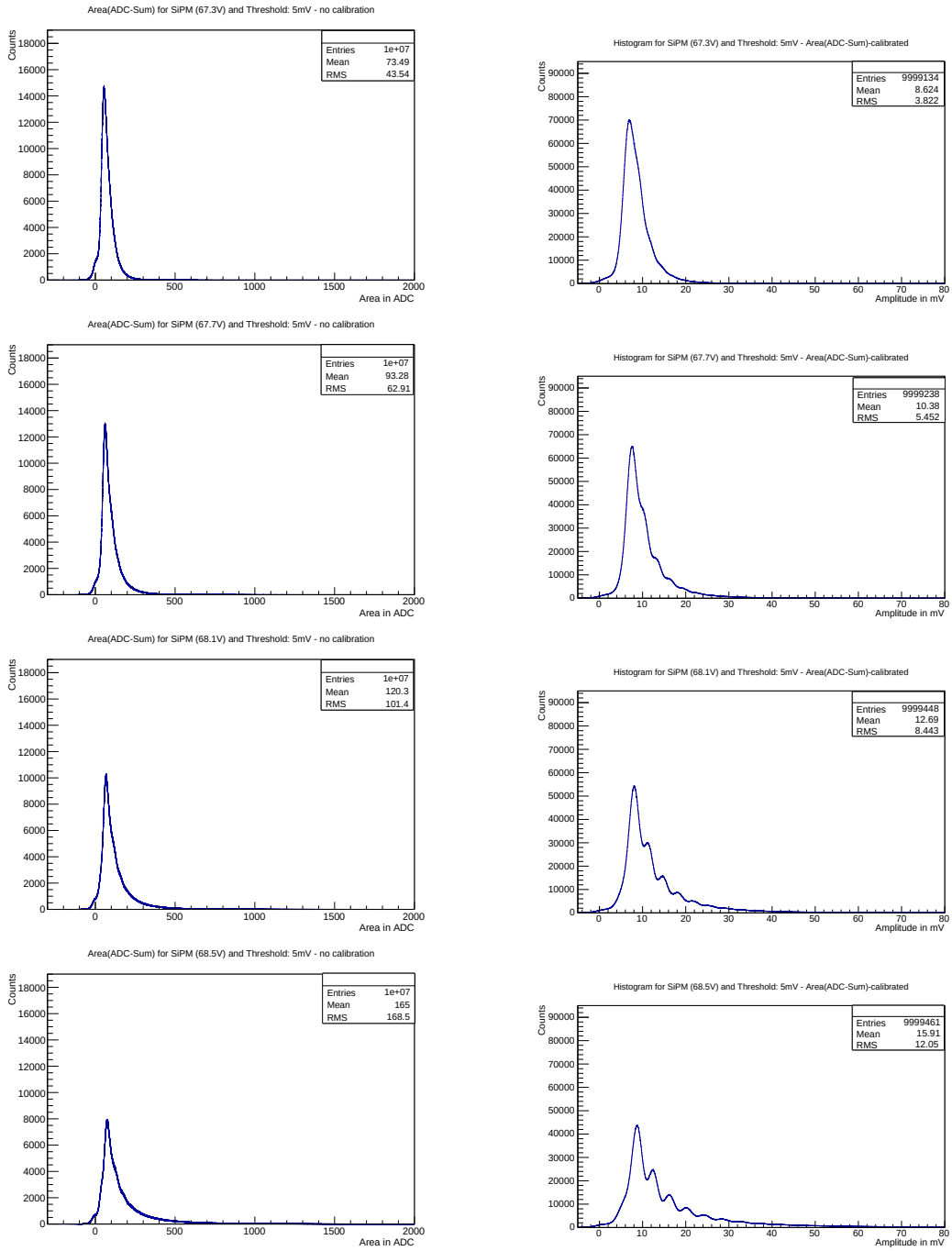

Figure 57: Area scan on SiPM signal (trigger: 5 mV) with TARGET ASIC and different SiPM voltages

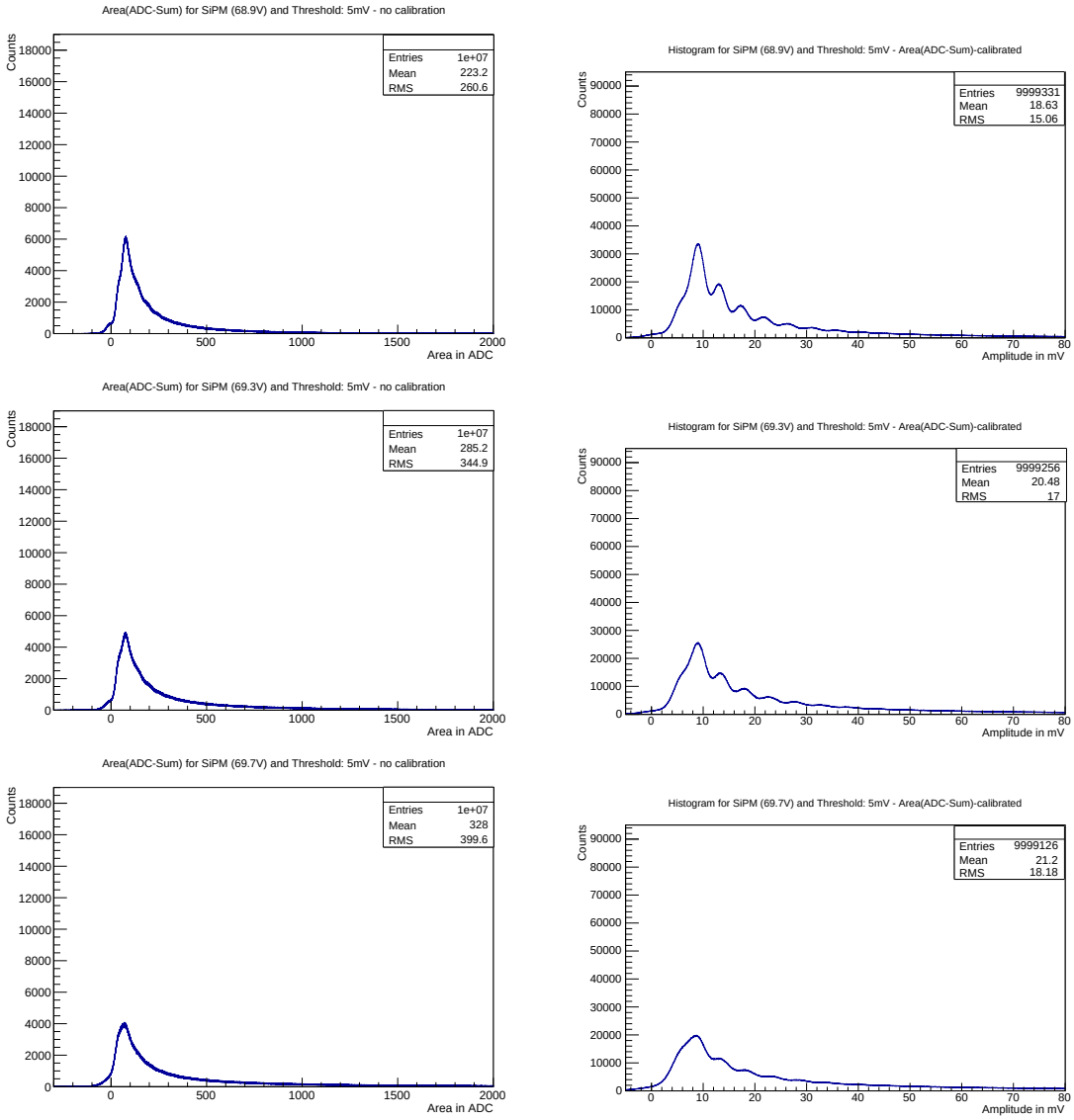

Figure 58: Area scan on SiPM signal (trigger: 5 mV) with TARGET ASIC and different SiPM voltages

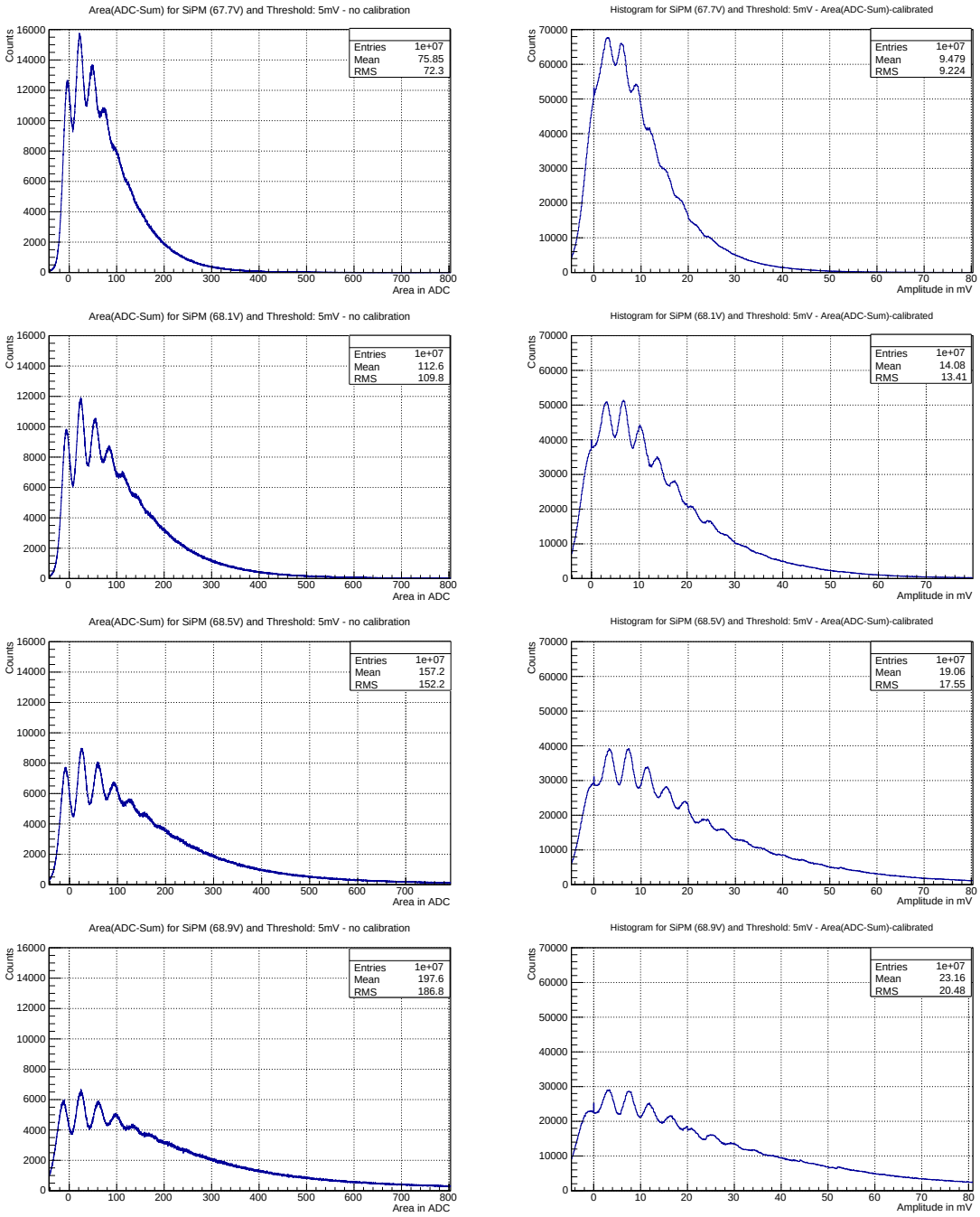

Figure 59: Area scan (trigger on laser pulse) on SiPM signal with TARGET ASIC and different SiPM voltages

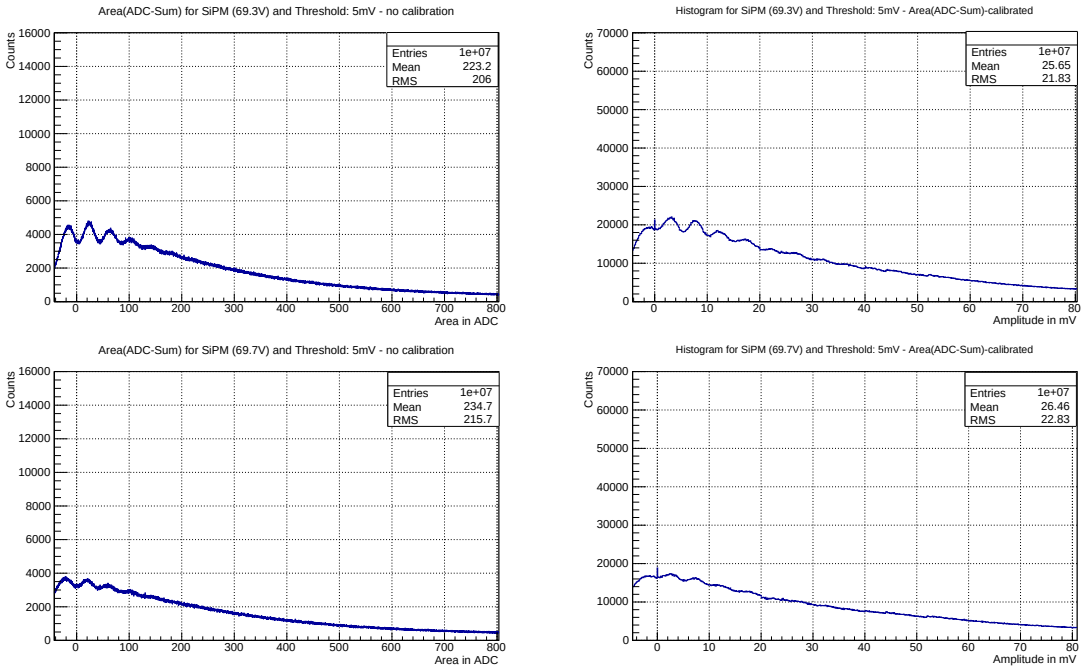

Figure 60: Area scan (trigger on laser pulse) on SiPM signal with TARGET ASIC and different SiPM voltages

A.6 Charge resolution

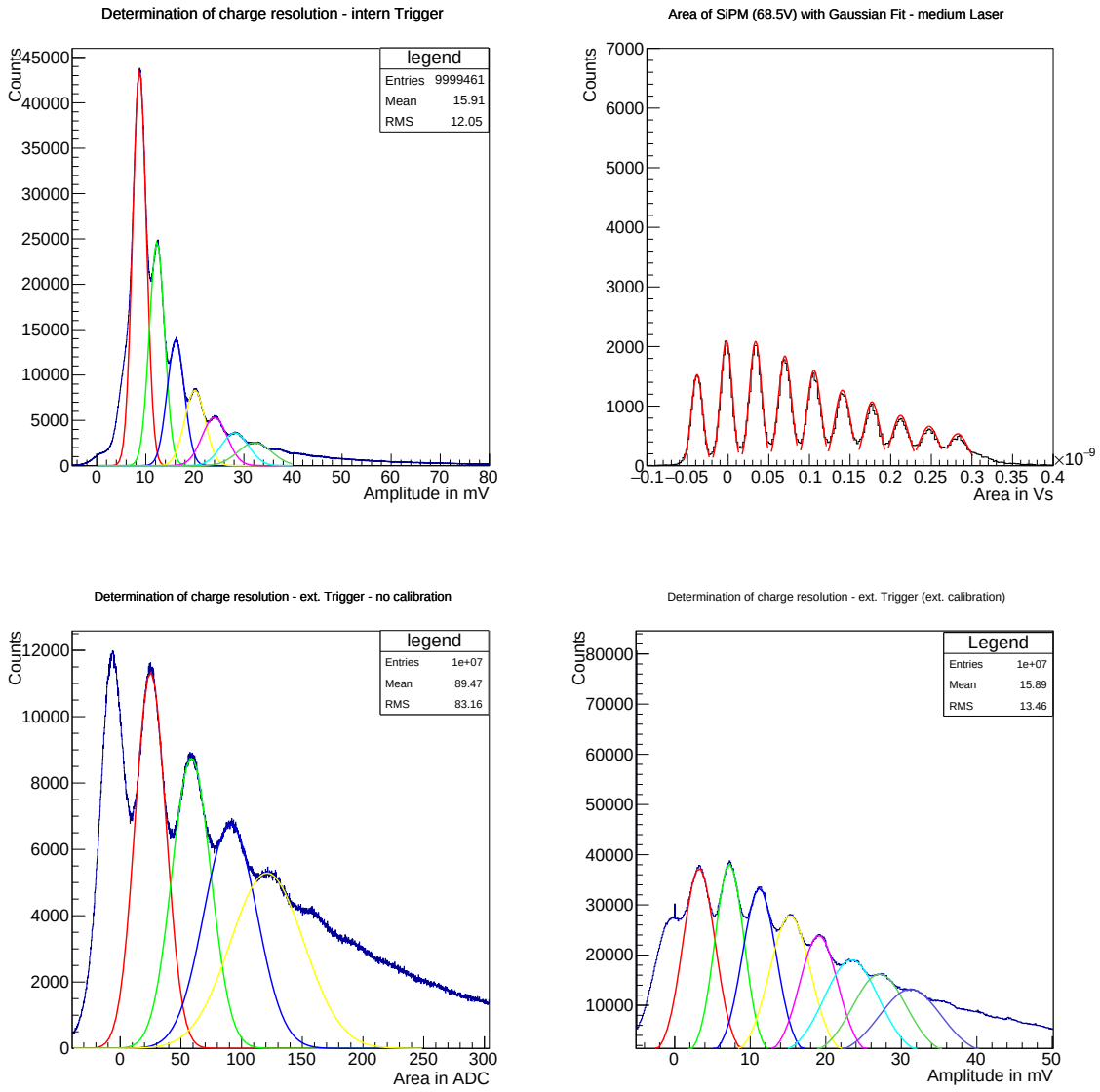

Figure 61: Single Gaussian fit to each p.e. peak. Oscilloscope (top right), TARGET with 5 mV threshold and area calibration (top left), TARGET with trigger on laser pulse without (bottom left) and with area calibration (bottom right)

A.7 Gain

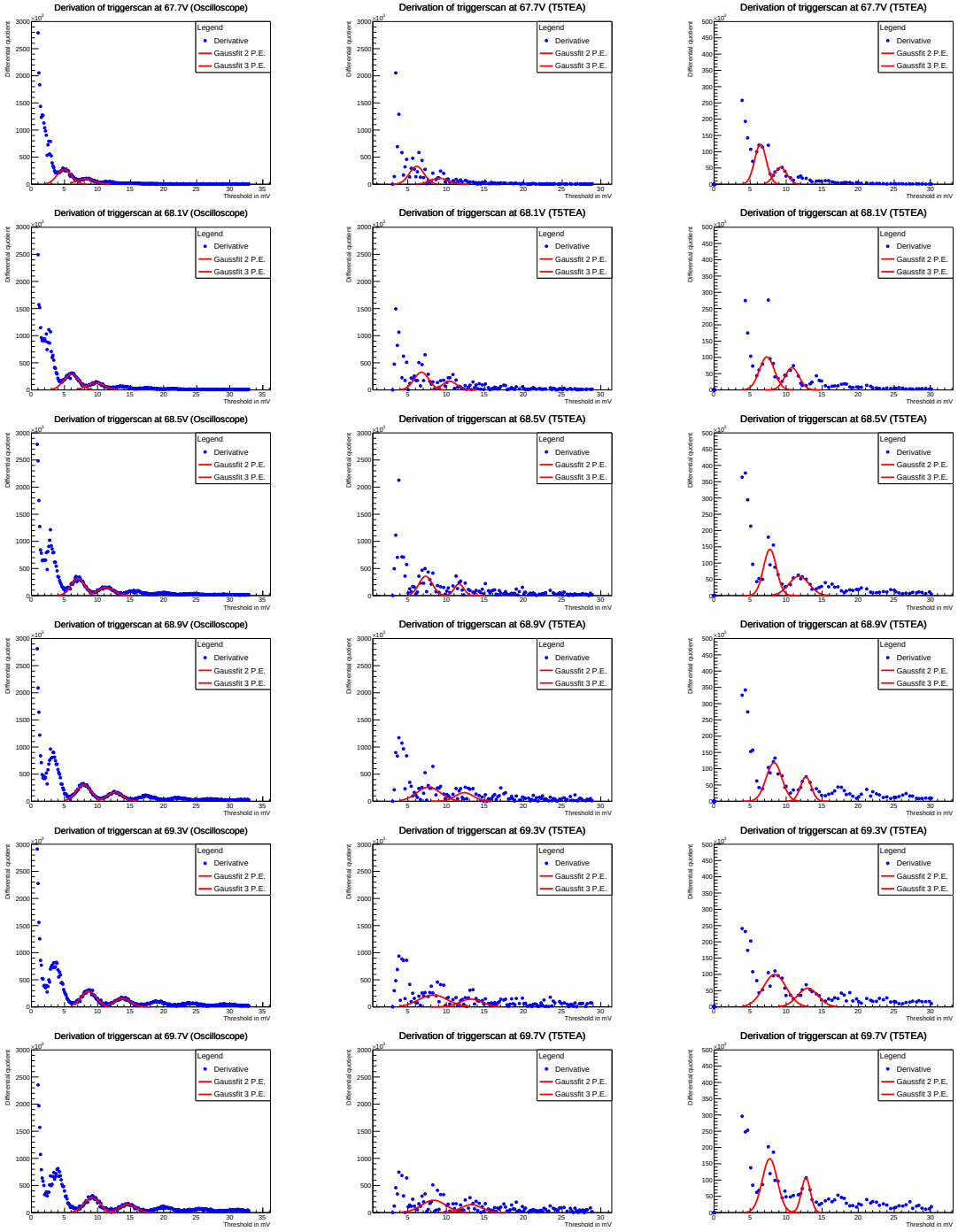

Figure 62: Derivative of triggerscan with oscilloscope (left), T5TEA (middle) and PMTref4-scan (right)

References

[1] M. Actis, G. Agnetta, F. Aharonian, et al. Design concepts for the Cherenkov Telescope Array CTA: an advanced facility for ground-based high-energy gamma-ray astronomy. *Experimental Astronomy*, 32:193–316, December 2011.

[2] M. Ackermann and M. Ajello. Detection of the Characteristic Pion-Decay Signature in Supernova Remnants. *Science*, February 2013.

[3] R. Blandford and W. East. Active Galactic Nuclei: The TeV Challenge. *ArXiv e-prints*, November 2015.

[4] The physics of gamma-ray sources from 4. January 2016. `http://www.mpe.mpg.de/~rod/GammaRaySources.pdf`.

[5] Atmospheric electromagnetic opacity from 4. January 2016. `https://upload.wikimedia.org/wikipedia/commons/3/34/Atmospheric_electromagnetic_opacity.svg`.

[6] Gamma-Strahlung from 4. January 2016. `https://www-zeuthen.desy.de/~kolanosk/astro0506/skripte/cosmics06.pdf`.

[7] T. C. Weekes and M. F. Cawley. Observation of TeV gamma rays from the Crab nebula using the atmospheric Cerenkov imaging technique. *Astrophysical Journal*, July 1989.

[8] Wolfgang Demtröder. *Experimentalphysik 3: Atome, Moleküle und Festkörper*. Springer–Verlag Berlin Heidelberg, fourth edition.

[9] Homepage of the CTA Observatory from 23rd November 2016. https://www.cta-observatory.org.

[10] A. Albert, S. Funk, T. Kawashima, et al. TARGET 5: a new multi-channel digitizer with triggering capabilities for gamma-ray atmospheric Cherenkov telescopes. *ArXiv e-prints*, July 2016.

[11] Johannes Schäfer. Parameter optimization of the T5TEA-ASIC for the Cherenkov Telescope Array.

[12] W. Benbow, A. N. Otte, f. t. pSCT Consortium, and t. CTA Consortium. Status of the Schwarzchild-Couder Medium-Sized Telescope for the Cherenkov Telescope Array. *ArXiv e-prints*, October 2016.

[13] D. Mazin, J. Cortina, M. Teshima, and t. CTA Consortium. Large Size Telescope Report. *ArXiv e-prints*, October 2016.

[14] S. Vercellone. The next generation Cherenkov Telescope Array observatory: CTA. *Nuclear Instruments and Methods in Physics Research A*, 766:73–77, December 2014.

[15] T. Montaruli, G. Pareschi, and T. Greenshaw. The small size telescope projects for the Cherenkov Telescope Array. *ArXiv e-prints*, August 2015.

[16] A. M. Brown, A. Abchiche, D. Allan, et al. The GCT camera for the Cherenkov Telescope Array. In *Society of Photo-Optical Instrumentation Engineers (SPIE) Conference Series*, page 99065K, July 2016.

[17] M. K. Daniel, R. J. White, D. Berge, J. Buckley, et al. A Compact High Energy Camera for the Cherenkov Telescope Array. *ArXiv e-prints*, July 2013.

[18] L. Tibaldo, J. A. Vandenbroucke, A. M. Albert, et al. TARGET: toward a solution for the readout electronics of the Cherenkov Telescope Array. *ArXiv e-prints*, August 2015.

[19] S. Funk, D. Jankowsky, H. Katagiri, et al. TARGET: A Digitizing And Trigger ASIC For The Cherenkov Telescope Array. *ArXiv e-prints*, October 2016.

[20] Jacqueline Catalano. Characterization of a custom designed trigger ASIC (T5TEA) for the Cherenkov Telescope Array.

[21] Datasheet of MSO-X 3054A oscilloscope. `http://literature.cdn.keysight.com/litweb/pdf/5990-6619EN.pdf?id=2002858`.

[22] Datasheet of Keysight 33611A Wavegenerator. `http://literature.cdn.keysight.com/litweb/pdf/5991-3272EN.pdf?id=2431617`.

[23] Judith Schneider. Charakterisierung von Siliziumphotomultipliern.

[24] S. Korpar, I. Adachi, H. Chagani, R. Dolenec, K. Hara, T. Iijima, P. Križan, S. Nishida, R. Pestotnik, and A. Stanovnik. Measurements of Cherenkov Photons with Silicon Photomultipliers. *Nuclear Physics B Proceedings Supplements*, 197:283–287, December 2009.

[25] schematics of avalanche photodiode from 4. January 2016. `https://upload.wikimedia.org/wikipedia/commons/9/92/APD2_German.png`.

[26] A technical guide to silicon photomultipliers (Hamamatsu) from 4. January 2016. `http://www.hamamatsu.com/eu/en/community/optical_sensors/articles/technical_guide_to_silicon_photomultipliers_sipm/index.html`.

[27] working principle of silicon photomultipliers (Ketek) from 4. January 2016. `http://www.ketek.net/products/sipm-technology/working-principle/`.

[28] explanation of occurrence of SiPM event from 4. January 2016. `http://www.hamamatsu.com/sp/hc/osh/hub_04e_12_tn2_figure01.gif`.

[29] Layout of Hamamatsu silicon photomultiplier from 4. January 2016. `http://www.hamamatsu.com/sp/hc/osh/hub_04e_12_tn1_figure01.jpg`.

[30] Daniel Fortmann. Untersuchung der Einzelphotonenauflösung von SiPMs mit der TARGET - Ausleseelektronik.

[31] Frank Sauerburger. Charakterisierung von Silizium Photomultipliern.

[32] Adrian Zink. Personal information.

[33] Interpolation from 13. January 2016. https://en.wikipedia.org/wiki/Interpolation.

[34] Extrapolation from 13. January 2016. https://en.wikipedia.org/wiki/Extrapolation.

Danksagung

Zum Abschluss möchte ich mich bei allen bedanken, die mir zur Seite gestanden und mich im Rahmen meiner Bachelorarbeit unterstützt haben. Besonders danken möchte ich dabei:

- **Prof. Dr. Stefan Funk** für die Vergabe dieses interessanten Themas.
- **Prof. Dr. Gisela Anton** für die Übernahme des Zweitgutachtens.
- **Adrian Zink** für die gute und angenehme Betreuung, die hilfreichen Tipps, wenn etwas nicht sofort funktioniert hat und das Korrekturlesen
- **David Jankowsky** für das Korrekturlesen und die hilfreiche Unterstützung.
- **Johannes Schäfer** für das Korrekturlesen und die Verbesserungsvorschläge.
- **Meinen Kollegen** und der Arbeitsgruppe für die produktive und trotzdem entspannte Arbeitsatmosphäre
- **Meiner Familie** für die Unterstützung während des gesamten Studiums und die Aufmunterung, wenn es mal Probleme gab.

Erklärung

Hiermit bestätige ich, dass ich diese Arbeit selbstständig und nur unter Verwendung der angegebenen Hilfsmittel angefertigt habe.

Erlangen, den 17. 1. 2017